

**INVESTIGATION OF LIQUID TRANSPORT IN  
MICRO AND NANOSCALE POROUS MEDIA AT  
DIFFERENT PORE TO THROAT SIZE RATIOS**

**A Thesis Submitted to  
the Graduate School of Engineering and Science of  
İzmir Institute of Technology  
in Partial Fulfillment of the Requirements for the Degree of**

**MASTER OF SCIENCE**

**in Energy Engineering**

**by  
Gülce KALYONCU**

**July 2017  
İZMİR**

We approve the thesis of **GÜLCE KALYONCU**

**Examining Committee Members:**

---

**Assist. Prof. Dr. Murat BARIŞIK**

Department of Mechanical Engineering, İzmir Institute of Technology

---

**Assoc. Prof. Dr. Erdal ÇETKİN**

Department of Mechanical Engineering, İzmir Institute of Technology

---

**Assist. Prof. Dr. Sercan ACARER**

Department of Mechanical Engineering, İzmir Katip Çelebi University

**13 July 2017**

---

**Assist. Prof. Dr. Murat BARIŞIK**

Supervisor, Department of Mechanical Engineering, İzmir Institute of Technology

---

**Assist. Prof. Dr. Ünver ÖZKOL**

Co-Supervisor, Department of Mechanical Engineering, İzmir Institute of Technology

---

**Prof. Dr. Gülden GÖKÇEN**

**AKKURT**

Head of the Department of Energy Engineering

---

**Prof. Dr. Aysun SOFUOĞLU**

Dean of the Graduate School of Engineering and Sciences

## ACKNOWLEDGEMENTS

I would like to express my most sincere appreciations to my advisor Assist. Prof. Murat BARIŐIK who has always had patience and a strong motivation to keep me on track. He has always shown me new horizons and made me benefit from his valuable academical experiences and knowledge. I appreciate every second that he has spent with me to take me even further, as a student and as a human being.

For his valuable contributions and sincere navigation on this study, I would genuinely like to thank Prof. Ali BEŐKÖK. And, I am also thankful to the Center for Scientific Computation at Southern Methodist University for giving us the opportunity to use their high-performance computing center, ManeFrame. I would also like to thank Assist. Prof. Ünver ÖZKOL, and Assoc. Prof. Erdal ÇETKİN for their beneficial recommendations and kind support throughout my period of studies in IZTECH.

As a part of MiNaEng Research Group, that I have always been glad to be a part of; I would like to acknowledge to some of my colleagues that I am thankful for. For their undeniable support and contributions; I would like to thank Safa SABET and Tümcen ŐEN as well as for their help building my theoretical knowledge and dominance on my area of interest. Also, I am thankful to Gökberk ÖZÇELİK for his support, and motivation during this tough period. I would also like to thank Megan BARIŐIK, for the kind help she has given, for technical writing and academic issues that I have encountered on the road.

We would like to thank The Scientific and Technological Research Council of Turkey (TUBITAK), co-funded by Marie Curie Actions under FP7 for support under the grant number TÜBİTAK 115C026.

To the ones that have been here for me for a long time of my life, I would like to express my sincere gratitude to my dear friends Aslıhan AŐIK, Ceren KAYMAZ, and Orçun TANRISEVER, who have always motivated me, and have shown me the bright sides of life, with their warm friendship and kind support, when I have been dealing with harsh conditions through this journey.

To the precious ones who have always with me no matter what; I would like to send my deepest thankfulness to my mother Pakize KALYONCU, my father Azmi KALYONCU, and my sister Çağla KALYONCU, since they have never given up believing in me, and they have always shown their limitless support and help in terms of

everything. It would be really challenging for me to finish this dissertation without their presence which I have always felt.

At last but not least, I would like to express my gratitude to Efecan PAKKANER who has never hesitated to help me whatever the conditions are, without even thinking a bit to give the priority to me. I would like to thank him for his endless support, valuable helps, infinite motivation and his precious love that makes my life better.

## ABSTRACT

### INVESTIGATION OF LIQUID TRANSPORT IN MICRO AND NANOSCALE POROUS MEDIA AT DIFFERENT PORE TO THROAT SIZE RATIOS

Extensive usage of micro/nanoscale porous media in various applications, require comprehensive understanding of fluid transport in those systems, such as in the unconventional oil-reservoirs, micro/nano-membrane technologies and lab-on-a-chip applications. The frequently employed transport calculations in literature do not consider any effects related to size or shape of the pore. Instead, dynamically similar flow systems assumed by the porosity of a given medium that an “ability of flow” definition named permeability is employed for a given solid/liquid couple based on the corresponding porosity. However, in such small-scales, liquid flow characteristics diverge from continuum behavior and non-equilibrium effects should be considered to estimate the transport. Furthermore, geometrical parameters of pore structures and networks should be considered, in addition to porosity, for a proper characterization. Hence, pore scale analyses of fluid flow were performed by solving Navier-Stokes equation numerically with finite element method in a representative elementary volume. Permeability values were calculated based on the Darcy’s Law, at different pore-to-throat-size ratios, porosities, and velocity slips whose range determined by a literature review. Permeability showed a strong dependence on pore-to-throat-size ratios, and slip conditions. Using the permeability of pores across a wide range of conditions, the Kozeny-Carman (KC) relation was re-considered. An extended phenomenological Kozeny Carman model to predict micro/nanoscale liquid transport as a function of porosity, pore-to-throat size ratio, and slip length was developed. The pore-to-throat-size ratio and slip effects were found substantial on transport, which was successfully predicted by developed model.

**Keywords and Phrases:** Velocity slip length, permeability, porosity, pore-to-throat size ratio, computational fluid dynamics

## ÖZET

### FARKLI GÖZENEK- BOĞAZ GENİŞLİĞİ ORANLARINDAKİ MİKRO VE NANO ÖLÇEKLİ ORTAMLARDA SIVI TAŞINIMININ İNCELENMESİ

Mikro ve nano ölçekli gözenekli ortamların, petrol rezervleri, mikro ve nano ölçekli membran teknolojileri ve çip üstü laboratuvarlar gibi çeşitli uygulamalardaki sık kullanımları, bu tür sistemlerdeki akış taşınımının iyi anlaşılmasını gerektirmektedir. Literatürde hali hazırda uygulanmış olan taşınım denklemleri, gözenğin boyut ve geometrisiyle ilgili özelliklerinin sıvı taşınımı üzerindeki etkilerini çoğunlukla dikkate almamaktadır. Bunun yerine, dinamik olarak benzer akış sistemleri ortamın gözenekliliği ile tahmin edilmiş ve “akma kabiliyeti” olarak adlandırılabilir geçirgenlik tanımı belirli bir sıvı/katı çifti için gözeneklilik temelinde uygulanmıştır. Ancak, bu gibi küçük ölçekli akışlarda sıvı taşınım özellikleri süreklilik davranışından uzaklaşmaktadır. Bu sebeple, akışkan ile duvar arasında oluşan dengesizlik etkileri akışkanın özelliklerini tahlil edebilmek için incelenmelidir. Ayrıca, akış taşınımını doğru karakterize edebilmek için, gözenekliliğin yanısıra gözenek yapılarının ve ağlarının geometrik parametreleri de hesaba katılmalıdır. Bu sebeple, akışkanın gözenek ölçeğindeki analizi, temel bir temsilci hacim içerisinde, Navier-Stokes denklemlerinin sonlu elemanlar yöntemi kullanılarak sayısal olarak çözülmesi ile gerçekleştirilmiştir. Literatürden elde edilen farklı kayma uzunluğu değerlerinde, farklı gözeneklilik ve gözenek-boğaz genişliği oranlarındaki geçirgenlik değerleri Darcy Yasası kullanılarak hesaplanmıştır. Sonuçlar, gözenekliliğin gözenek-boğaz genişliği oranlarına ve kayma etkilerine bağlı olduğunu ortaya koymuştur. Bu geniş aralıkta elde edilen geçirgenlik değerleri kullanılarak, Kozeny Carman (KC) ilişkisi tekrar incelenmiştir. Mikro ve nano ölçekli ortamlarda sıvı taşınımını tahmin edebilmek amacıyla, gözeneklilik, gözenek-boğaz genişliği oranı ve kayma etkilerine bağımlı ve Kozeny Carman ilişkisinin bir uzantısı olan olgusal bir model geliştirilmiştir. Gözenek-boğaz genişlik oranı ve kayma etkilerinin, geliştirilen model aracılığıyla başarılı bir şekilde tahmin edilen geçirgenlik değerleri üzerinde azımsanmayacak etkilere sahip olduğu gözlemlenmiştir.

**Anahtar Kelimeler ve Deyimler:** Kayma hızı uzunluğu, geçirgenlik, gözeneklilik, Kozeny- Carman denklemi, hesaplamalı akışkanlar dinamiği

# TABLE OF CONTENTS

LIST OF FIGURES .....	ix
LIST OF TABLES .....	xi
LIST OF SYMBOLS .....	xii
CHAPTER 1. INTRODUCTION .....	1
CHAPTER 2. LITERATURE REVIEW .....	6
2.1. Porous Medium and Their Applications .....	6
2.2. Kozeny Carman Equation and Kozeny Carman Constant.....	8
2.3. Effect of Throat Size on Permeability .....	15
2.4. Permeability of Small Scale Porous Medium .....	17
2.5. Micro/Nanoscale Liquid Transport.....	18
2.5.1. Slip velocity and Slip Length .....	19
2.5.2. Effect of Wettability .....	23
CHAPTER 3. FORMULATION OF THE PROBLEM .....	27
3.1. Volume Average Method and Pore Scale Method .....	27
3.2. Darcy and Kozeny-Carman Equations .....	29
3.3. Governing Equations and Boundary Conditions for Determination of Permeability .....	31
CHAPTER 4. SOLUTION METHOD .....	35
4.1. Numerical Procedure .....	35
4.2. Computational Details .....	35
4.3. Mesh Independency Tests.....	36

CHAPTER 5. RESULTS AND DISCUSSION .....	38
5.1. Calculations of Permeability.....	38
5.2. Calculations of Kozeny Carman Constant.....	50
5.3. Extend of Kozeny Carman Model for Liquid Slip .....	53
CHAPTER 6. CONCLUSION.....	62
REFERENCES .....	64



## LIST OF FIGURES

<u>Figure</u>	<u>Page</u>
Figure 2.1. Slip length values measured at different wetting conditions. ....	26
Figure 3.1. Microscopic control volume in a porous structure .....	28
Figure 3.2. Schematic view of the considered porous media, and REV which drawn with the dashed lines (right). ....	32
Figure 4.1. Variation of the (a) velocity profile, (b) enlarged view of the velocity profile at the specific location in y direction, (c) evaluated pressure drop values with different mesh densities (d) dimensionless permeability with different mesh densities.....	36
Figure 5.1. Representation of computational domain with geometrical notations. ....	39
Figure 5.2. The change in the non-dimensional pressure drop values with respect to Reynolds number for both slip and no slip flow cases. ....	39
Figure 5.3. Representation of REV when aspect ratio is equal to 1 with different porosities of (a) 0.1, (b) 0.2, (c) 0.3, (d) 0.4, (e) 0.5, (f) 0.6, (g) 0.7, (h) 0.8, and (i) 0.9 .....	41
Figure 5.4. Validated results of dimensionless permeability values with reference studies.....	42
Figure 5.5. Pressure contours and streamlines of REV for a constant porosity of 0.4 and with different $R_{pt}$ and slip conditions. ....	44
Figure 5.6. Representation of velocity profile with contours by comparing no slip and slip conditions with 5 nm and 50 slip length results for a constant porosity of 0.4 and different values of $R_{pt}$ and $L_s$ .....	45
Figure 5.7. Representation of streamlines and pressure contours in the considered domain for a specified $R_{pt}=4$ with slip and no slip boundary conditions. ...	47
Figure 5.8. The variation in dimensionless pressure gradient and dimensionless permeability values with different porosities. (Figures (a&b), (c&d), and (e&f) represent no slip, slip with 5 nm and 50 nm slip length results, respectively.).....	49
Figure 5.9. Permeability-porosity relation with different slip conditions and pore to throat size ratio. (a) $R_{pt}=4$ , and (b) $R_{pt}=10$ .....	50

Figure 5.10. Change in $C_{KC}$ with porosity for different $R_{pt}$ values at (a) no slip, (b) $L_s=5$ nm, (b) $L_s=50$ nm. ....	51
Figure 5.11. Comparison between the results of proposed model and Kozeny-Carman equation (a)no slip, (b) $L_s=5$ nm, and (c) $L_s=50$ nm. ....	53
Figure 5.12. Permeability variation with respect to slip length ( $L_s$ ) for (a) $R_{pt}=10$ (b) $R_{pt}=6.66$ (c) $R_{pt}=5$ , (d) $R_{pt}=4$ , and (e) $R_{pt}=2.6$ .....	54
Figure 5.13. Variation in the non-dimensional permeability values and slip coefficient for (a) $R_{pt}=10$ , (b) $R_{pt}=5$ , (c) $R_{pt}=4$ , (d) $R_{pt}=2.6$ . ....	55
Figure 5.14. The relation between non-dimensional permeability and slip coefficient and the fitting trend lines with different $R_{pt}$ values as (a) $R_{pt}=10$ (b) $R_{pt}=5$ (c) $R_{pt}=4$ , and (d) $R_{pt}=2.6$ . Dashed lines represent the fitting trend line. .	58
Figure 5.15. Fitting functions of coefficients A (left) and B (right) as a function of porosity for a specific $R_{pt}$ .....	59
Figure 5.16. Coefficients in Eq. (5.10) and (5.11) as a function of $R_{pt}$ .....	60
Figure 5.17. Comparison between the simulation results and results of proposed model for permeability as a function of slip coefficient with (a) $R_{pt}=10$ , (b) $R_{pt}=5$ , (c) $R_{pt}=4$ , (d) $R_{pt}=2.6$ . Notation of (C) and (Eq. 5.16) denote the results of numerical computations, and calculations results of the proposed model, respectively .....	61

## LIST OF TABLES

<b><u>Table</u></b>	<b><u>Page</u></b>
Table 2.1. Models in the existing studies which relates tortuosity ( $\tau$ ) and porosity ( $\epsilon$ )..	10
Table 2.2. Relations derived between permeability and porosity .....	13
Table 2.3. The suggested relations for determination of Kozeny Carman constant .....	15
Table 2.4. Summary of the slip lengths and the slip coefficient ( $\beta$ ) based on corresponding conduit sizes from the literature. ....	21
Table 2.5. Summary of slip length measurements with corresponding contact angle values. ....	24
Table 5.1. Lower and upper limits of porosity values for determined pore to throat size ratios.....	48
Table 5.2. The empirical coefficients for the evaluation of Kozeny Carman constant...	52

## LIST OF SYMBOLS

D	Size of square particle	m
H	Representative Elementary Volume (REV) dimension	nm
K	Permeability	m <sup>2</sup>
p	Pressure	Pa
R <sub>pt</sub>	Pore-to-throat size ratio	
Pr	Prandtl number	
Re	Reynolds number	
Kn	Knudsen number	
u	Velocity in x direction	m/s
$\vec{u}$	Velocity vector	m/s
L <sub>s</sub>	Slip length	m/s
v	Velocity in y-direction	m/s
U	Non-dimensional velocity in Eq. (5.7)	
V	Volume	m <sup>3</sup>
KC	Kozeny Carman relation	
C <sub>KC</sub>	Kozeny Carman constant	

### Greek Letters

$\varepsilon$	Porosity	
$\theta$	Contact angle	deg.
$\beta$	Dimensionless slip length	
$\mu$	Dynamic viscosity	N.s/m <sup>2</sup>
$\nu$	Kinematic viscosity	m <sup>2</sup> /s
$\rho$	Density	kg/m <sup>3</sup>
$\phi$	Any parameter	
$\tau$	Tortuosity	

### Subscripts

f	Fluid
s	Solid, slip
w	Wall
p	Particle
xx	Longitudinal
yy	Transverse

# CHAPTER 1

## INTRODUCTION

A porous medium is a structure which includes stable solid parts and the empty spaces to provide fluid flow. The solid part of the porous media called as solid matrix, and the gap between the solid particles can be named as void space. There exists a plethora of examples about porous media in nature, and in various applications in the modern world. For instance, kidneys, lungs, bones, soil, limestone, bread, and even human hair serve as examples for natural porous media. Water purification systems, usage of heterogeneous catalysts in the reactors, liquid chromatography applications, membranes, biochemical applications, tissue engineering, biological membranes, well drilling, and hydraulic fracturing through ultra-tight shale gas and oil reservoirs are some examples of porous media application area in the industry.

From the porous nature of the medium itself, the fluid flow inside can be difficult to characterize in a three-dimensional system and these characterizations could be crucial for determining the outcomes of the applications. Two main approaches exist to analyze flows in porous media, Pore Scale Method (PSM), and Volume Average Method (VAM). Using PSM provides very precise results of prediction of transport behavior, since it presents a solution for transport by considering every pore in the medium. However, due to the inherent heterogeneous and complex features of porous media, evaluation of velocity and temperature with the pore scale approaches is not very easy. Hence, the need for different approaches to characterize flow behavior easier in porous medium is required. In order to overcome the challenges, that occur from characterizing such a complex flow domain, VAM approach is mostly preferred as it neglects the discontinuity caused by the solid network matrix. Implementation of this method is accomplished by taking volume integral of continuity, momentum, and energy equations which enable us to calculate volume averaged velocity, pressure and temperature values of the system. The application of volume averaged method on flow equations yields to addition of several more parameters presenting VAM transport behavior such as permeability. Numerous studies are concentrated on the evaluation of volume averaged parameters for porous media with distinctive characteristics.

One of the key aspects for characterizing porous media is permeability which physically defines the ease of the flow through pores. Permeability can be classified as flow conductivity, and it is directly influenced by the structure of the medium. Due to this, determination of permeability by quantitative evaluation is highly complicated. Moreover, measurement techniques for permeability are also costly (Gao and Hu, 2013). Despite the mentioned challenges, evaluation of permeability is essential for characterizing transport behavior through porous medium. Henry Darcy had conducted an experiment which was based on a water filtration procedure applied through sand beds. With the output of this experiment, he observed that, flow rate and pressure are linearly changing with a constant value of flow conductivity- which was later described as permeability (Darcy, 1856). The relation was based on the assumptions that fluid flow inside the pores was homogenous and isotropic and the system was resolved by taking an average of the separate pores. This empirical correlation is valid for creeping flow, namely  $Re < 1$ . Darcy's Law was extended by several researchers. In order to consider the boundary effects, Brinkman added the diffusion term to Darcy's equation; while for large velocities, Forchheimer indicated that the pressure gradient as a consequent result of specific flow rate that was obtained via Darcy's Law is less than what Forchheimer evaluated. Therefore, he added a coefficient to Darcy's Law with the consideration of inertial and viscous effects (Liu and Masliyah, 1996).

Since measuring permeability is rather complex, it was attempted to be derived as a function of a more reachable parameter, such as porosity. For that, Kozeny proposed a relation which defines permeability as a function of porosity. Briefly, he defined a system composed of a stack of capillary tubes that have the same diameter and length, with a fluid flowing within. Carman, then, improved this relation. Subsequently, the Kozeny-Carman equation (KC) was proposed that contains a constant named after Kozeny, which briefly gathers the effects of flow path, shape of the particles and their connections together. In KC relation, this mentioned constant was simply stated as 5 (Kozeny, 1927; Carman 1937; 1939). Researchers have tried to determine Kozeny Carman constant ( $C_{KC}$ ) by both experiments and numerical calculations using different methods such as lattice Boltzmann Method (LBM), Pore Network Modelling (PNM), and Computational Fluid Dynamics (CFD) simulations. All these techniques have both advantages and disadvantages and detailed information can be found elsewhere (Khabbazi et al., 2013).

One of the key factors determining the permeability is the connectivity of the pore network. Generally, KC relation is correlated only by taking porosity into account. Multiple researchers emphasized the importance of the pore network structure and concluded that it has a dominant effect and should be included in the correlations derived based on KC relation. More recently, Ozgumus et al. proposed a relation for the calculation of  $C_{KC}$  as a function of pore to throat size ratio, to improve the validity of KC relation, to be used across a broad range of geometrical aspects (Ozgumus et al., 2014).

Another dominant mechanism affecting permeability is the non-equilibrium developing in fluid dynamics due to the very small scale of porous systems. Many applications are based on pore sizes in the range of micro/nanoscales where liquid dynamics diverge from the continuum behavior. Hence, depending on the pore sizes, the flow characteristics differ from the conventional porous medium transport behavior. In such cases, permeability values obtained from KC equations for a specific porosity should be corrected, in order to add the scale effects, which are not considered by the Darcy equation. Using existing available permeability for a given porosity and pore-to-throat-size ratio underestimates the transport observed at micro/nano-scales. A general first description for small scale effects was developed by Klinkenberg as a correction to Darcy's law, in order to consider so-called slip effects in the case of gas transport (Klinkenberg, 1941). Nevertheless, for the liquid flow, non-equilibrium effects have not been considered in the permeability characterizations for micro/nanoscale liquid flows.

There is a great demand from the most current technologies (i.e. lab-on-a-chip, nano-membranes, and water and environmental engineering applications) to understand liquid transport at micro/nano-scales. For example, in petroleum engineering, flows through the nanopores of shale have received significant attention lately (Singh and Javadpour, 2016; Afsharpoor and Javadpour, 2016; Cui et al., 2017; Jin et al., 2017). There have been a couple of attempts proposing the addition of liquid slip effects into the permeability calculations to accurately estimate the permeability of liquid transport in micro/nanoscale porous media.

In order to accurately describe transport behavior through micro/nanoscale porous media, non-equilibrium effects should be characterized. At micro/nano levels, the interactions between fluid and surface become dominant and create non-equilibrium behaviors in fluid dynamics so that classical continuity-based theories cannot resolve the heat and mass transport. Whereas, the non-equilibrium behavior develops differently in gas and liquid flows. Effects of the non-equilibrium behavior are observed in the near-

wall region. Possible solution procedure should be determined according to the extent of this near-wall non-equilibrium region into the entire flow domain.

The micro/nanoscales dynamics developing in case of a gas flow is a well-studied subject due to the convenient calculations provided by Kinetic Theory (KT) and Molecular Dynamics (MD). Basically, the Knudsen number ( $Kn = \lambda / D_H$ ) calculated as the ratio of gas mean free path ( $\lambda$ ) to the characteristic height of confinement ( $D_H$  is the hydraulic diameter) provides an understanding of non-equilibrium gas dynamics, while the B parameter ( $B = L_f / D_H$ ) calculated as the ratio of surface molecular force penetration depth to characteristic height of confinement considers the effect of surface forces which are dominant at nano-scales (Barisik and Beskok, 2014). However, small scale effects on liquid flows are not that simple to estimate. This deficiency is mostly caused by the complex momentum exchange behaviors of liquid molecular system in which the collision dynamics cannot be calculated using Kinetic Theory of gases due to the high density. Hence, the Kn number cannot be defined for liquids and related theories and solution procedures cannot be applied. There are multiple studies defining Kn and employing KT based solutions such as Maxwell defined velocity slip and temperature jump models as a function of Kn for liquid flows (Mirramezani and Mirdamadi, 2012; Rashidi et al., 2012; Matin et al., 2013; Bardia et al., 2016) as well as for characterization of nanofluids (liquids containing nanoparticles) (Buongiorno, 2006; Hooman et al., 2009; Hooman and Ejlali, 2010; Akbarinia et al., 2011; Yang et al., 2015) which are misleading researchers to an incorrect physical interpretations of liquid flows at micro/nanoscale.

On the other hand, there are no existing theories to generally characterize liquid non-equilibrium behaviors and their length scales. The molecular surface forces and adsorption develop different mechanisms than gas state. Basically, non-equilibriums are observed at the liquid/solid interface momentum and energy exchange coupling, as well as at the near interface liquid dynamics. Velocity slip and temperature jump develops at the interface between surface and liquid while density layering and electric double layer are two major complications forming in liquid at near interface. But, the length scales of near interface non-equilibrium regions are very small such that its contribution is negligible for even very small confinements. Hence, over a certain dimensional limit defining an updated boundary condition for an overall consideration of the non-equilibrium effects can be performed.



Multiple researchers attempted to solve micro/nanoscale liquid flows with the velocity slip boundary conditions in order to include non-equilibrium effects. The idea about the velocity slip was first proposed by Navier (Navier, 1823). According to the Navier's well known boundary conditions, the velocity at the surface  $v_{slip}$ , is proportional to shear stress at the wall (Gad el Hak, 1999).

$$v_{slip} = L_s \left. \frac{dv}{dy} \right|_w \quad (1.1)$$

Where  $\left. \frac{dv}{dy} \right|_w$  is the velocity gradient at the wall, and  $L_s$  is the slip length. Slip length measures the velocity slip as a fictitious distance at which the velocity extrapolates to the value of zero. Slip length is expected to depend on properties of solid and liquid couples as well as on the flow dynamics.

The purpose of the current study is to understand liquid flow through micro/nanoscale porous media with different pore -to-throat size ratios by considering the slip effects on permeability. Permeability values will be calculated based on Darcy's Law and the comparison between no-slip and slip flow cases will be examined, and Navier-Stokes equations with slip boundary conditions will be solved numerically by using Finite Element Method (FEM). For such a case, velocity slip measurements from existing literature will be summarized and results will be normalized by the characteristic length of the corresponding flow domain to develop a possible range of slip coefficients that can be found in Chapter 2. KC equation will be applied on the permeability results calculated at different porosity and pore-to-throat size ratios. An extended phenomenological KC model to predict micro/nano liquid transport as a function of porosity, pore-to-throat size ratio, and slip length will be developed.

The outline of this study can be summarized as follows; In Chapter 2, a comprehensive literature survey on porous media applications, porous transport calculation methods, and micro/nanoscale liquid transport will be given. In Chapter 3, a formulation of the problem will be discussed. In Chapter 4, the computational domain used for numerical calculations, and related details will be presented. In Chapter 5, results based on the solution of fully developed flow through Representative Elementary Volume will be revealed in terms of porosity, pore-to-throat size ratio, and permeability for both slip and no slip flow, and these results will be interpreted in detail. Lastly, in Chapter 6, the study will be summarized and appropriate conclusions will be made.

## CHAPTER 2

### LITERATURE REVIEW

In this section, the knowledge which gained from the literature about the application areas of porous media, porous transport calculation methods, a brief review about permeability calculations on Kozeny Carman relation (KC), and the geometrical effects on the permeability are presented. Additionally, to investigate the non-equilibrium behavior of liquid flow in micro/nanoscale porous structures, an extensive literature review of micro/nanoscale liquid transport characteristics is given in terms of slip velocity, slip length and wettability characteristics of surface which have crucial role on the porous media transport characteristics.

#### 2.1. Porous Media and Their Applications

A porous medium can be identified as the combination of a unified arrangement of solid particles which have random dimensions and different forms. Area of the liquid or gas flow is often defined as the empty space (or void space). The use of porous media has been encountered in numerous areas, including chemical and petroleum engineering (shale reservoirs and alternative oil resources, heterogeneous catalysis, combustion phenomena, chromatography, separation and purification technologies, filtration, etc.) environmental sciences (wastewater and groundwater treatment, hydrology, marine microbiology, etc.), biological and biomedical applications (drug delivery, perfusion bioreactors and tissue engineering, regenerative medicine), energy systems (fuel cells, electrochemistry, nuclear waste disposal) and so on. Due to those diverse application areas that use porous transport theory, characterization of fluid flow through porous media has gained a significant attraction.

Due to the severe diminishment in the water sources, obtaining fresh water in alternative ways has become a prominent topic. To resolve this issue, desalination process, the most common technique used for obtaining freshwater by filtering sea water, needs to be improved. To accomplish this, nanomembranes have been investigated in detail by several researchers to increase the rate and efficiency of desalination process.

(Phillip et al., 2006; Tanugi and Grossman, 2012;2014; Thomas et al., 2014; Heiranian et al., 2015) Based on porous media research, Baban and Seymour conducted an important study which can open the pathways to overcome possible obstacles on tumor permeability, in order to further examine cancer drug delivery and enhanced permeability and retention effect applicable on tumor cells (Baban and Seymour, 1998). Khaled and Vafai investigated some fundamental transport models in porous media including; Darcy, Brinkman, and Forchheimer models. The specific usage areas of those models are reviewed in detail. The aforementioned models were found to be promising to characterize some physiological phenomena, including diffusion of body fluids in tissues, blood flow characteristics in tumors, and tissue generation. Also, for biological tissues, Darcy and Brinkman models for momentum transport and thermal equilibrium for energy transport were deemed appropriate to analyze the biological applications listed as tissue regeneration and drug and nutrient delivery to neural cells (Khaled and Vafai, 2003).

Rather different than the proposed areas, Khalili et al. have innovatively attempted to adapt those transport ideas into marine biology applications. For example, they numerically investigated porous media with lattice Boltzmann method (LBM), and they provided a comprehensive review about the recent applications of porous transport in marine microbiology, as well as for potential future implementations (Khalili et al., 2010).

From an environmental engineering point of view, one of the cornerstone studies about this area, the Brinkman model and existing capillary model were compared in terms of permeability predictions for deep bed filtration by Payatakes and his colleagues (Payatakes, 1974). Also, several other researchers focused on improving water treatment processes (Discacciati et al., 2002; Layton et al., 2003; Discacciati and Quarteroni, 2009). It was pointed out that the existence of suspended solids in the flow through porous medium, results in blockage of flow area, since some of those suspended solids have nearly the same size and/or are greater than pores. For such a case, permeability of the system is gradually decreased, and clogging occurs which eventually prevents particles from migrating and the injection process is negatively affected. As a result, a model was proposed based on various flow theories to predict the possible fluctuations in permeability to regulate the particle migration and flow characteristics of the porous systems (Liu et al., 2017).

In our modern world, the exploitation of fossil fuels and depletion of energy sources comes with its own problems that threaten nature every day. As part of their investigations, the yield of combustion phenomena was examined in the presence of a

porous medium. Mujeebu's study deals with the performance boost of combustion of hydrocarbons, using porous media as the reaction medium. Specifically, thermal efficiency and heat and mass diffusion properties were attempted to be enhanced with the increase in the mass and heat transfer area of the specified porous medium. A further comprehensive review about porous media combustion can be found in the mentioned study. (Mujeebu et al., 2009).

The studies above are some of the preliminary examples of porous media usage in various modern world applications. More specifically, the diminishment in the natural resources increases the importance of unconventional type reservoirs, including rocks, shale reservoirs, and oil pockets (Cui et al., 2017; Appiah et al., 2013; Afsharpoor and Javadpour, 2016; Naraghi and Javadpour, 2015; Wang and Sheng, 2017). However, the topographies of the mentioned sources possess nanoscale pores which have different transport behavior due to the small scale within them. As a result, implementation of conventional no-slip boundary conditions through such nanoscale porous media underestimates the permeability results, and yields to misleading interpretations of the process. To prevent that, some apparent permeability models obtained via solution with slip boundary condition have been developed. Those models are going to be mentioned in the further paragraphs in detail.

## **2.2. Kozeny Carman Equation and Kozeny Carman Constant**

Transport in porous media can be characterized by evaluating the permeability of the system. However, the difficulty of measurement of permeability values led researchers to develop models that can predict permeability as a function of parameters of porous systems that are comparatively easy to measure, such as porosity. Kozeny suggested a theory about a possible relation between permeability and porosity. During the development of this theory, porous media was assumed as a package of capillary tubes that have identical length and diameter. For the incompressible, laminar and steady state Newtonian flow, solution of Navier Stokes equation was obtained (Kozeny, 1927). After Kozeny's proposed derivation, Carman re-studied Kozeny's proposed relation by stating that Kozeny parameter varies in accordance with the porous medium (Carman, 1937; 1939), and finally Kozeny-Carman relation (KC) is obtained and related permeability ( $K$ ) with porosity ( $\epsilon$ ) can be seen in Eq. (2.1) (Xu and Yu, 2008).

$$K = \frac{\varepsilon^3}{C_{KC}(1-\varepsilon)^2 S^2} \quad (2.1)$$

Where  $C_{KC}$  is Kozeny Carman constant (or sometimes called as Kozeny parameter, or Kozeny constant) which identified as a function of geometry of the flow domain, and  $S$  is the specific surface area of the porous media.

KC equation relating the permeability with porosity has been found as a quite practical way to estimate permeability of porous media. It is widely used and provides good results in many cases (Adler, 1988; Thies-Weesie and Philipse, 1994; Heijs and Lowe, 1995; Parada, 2009). Nevertheless, KC relation becomes inadequate for estimating permeability values since this equation does not consider some structural properties of complex geometries. For a better characterization and estimation of porous transport, some other geometrical parameters should be considered in addition to porosity. Therefore, in order to obtain more universal relation, researchers have been trying to develop new correlations based on KC equation.

Among those parameters, an important geometry dependent parameter; tortuosity is mostly considered by several researchers (Lin et al., 1992; Xiao et al., 2012; Chen et al., 2015; Khabbazi et al., 2016, Liu et al., 2016). Basically, tortuosity defines the complexity of the path that fluid follows through porous structures (Khabbazi et al., 2015). The parameters that generate the complexity such as tortuosity are considered generally in fractal geometries. Fractal geometries provide more realistic considerations in order to investigate flow characteristic in porous media. As a solution technique, the fractal model has been performed in several studies which identified the significant role of the structural effects on permeability. Further information about the impact of fractal geometry techniques which have been found to be an efficient way to understand the transport behavior in complex porous medium can be found elsewhere (Xu, 2015).

Besides its significant role on the permeability predictions, since obtaining tortuosity values is rather complicated, some researchers have proposed tortuosity definitions based on porosity. Koponen and his colleagues evaluated the permeability of a porous medium with randomly distributed solid rectangular shapes by using LBM. They compared their simulation those obtained by adjusted KC equation by replacing porosity term with the effective porosity. The porous flow parameters, including effective porosity and tortuosity were investigated as a function of porosity. Results belonging to the revisited KC equation and numerical simulations agreed well (Koponen et al., 1996).

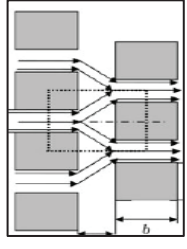
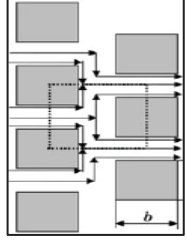
Following the previous study, the model was re-considered since the previously proposed model cannot yield a solution for the very near region of percolation threshold (Koponen et al., 1997). Boving and Grathwohl derived a relation between tortuosity and porosity by conducting an experimental study. Firstly, they measured the porosity and tortuosity values of limestone and sandstone individually, then derived a correlation based on those results which can be used specifically for the organic contaminants in sedimentary rocks with a common morphological form. (Boving and Grathwohl, 2001). Similarly, for a creeping flow in a rectangular shape pore structures, Yu and Li have proposed an approximate model to describe the tortuosity as a function of porosity without using an empirical constant. In their study, they investigated the porous medium where fluid follows a realistic path where the period of streamlines changes and an idealized path which can be considered for un-overlapped particles (Yu and Li, 2004). By using LBM, Matyhka et al. showed the relation between porosity and tortuosity numerically for pore structures which are randomly distributed, and are in the same shape with equal sizes. (Matyhka et al., 2008). Similarly, another tortuosity-porosity relation was derived by Khabbazi and his colleagues for the porous medium as the composition of rectangular particles. The results were procured by LBM for different aspect ratios, and it was revealed that there is an inverse relation between tortuosity and porosity. They also indicated that as the porosity increases, the role of aspect ratio on the tortuosity decreases, therefore for low values of porosity, the effect of aspect ratio on tortuosity should be investigated. The summary of the suggested correlations is displayed in Table 2.1.

Table 2.1. Models in the existing studies which relates tortuosity ( $\tau$ ) and porosity ( $\varepsilon$ )

Koponen et al., 1996	$\tau = 0.8(1 - \varepsilon) + 1$ For $0.4 \leq \varepsilon \leq 0.9$
Koponen et al., 1997	$\tau = 1 + 0.65 \frac{(1 - \varepsilon)}{(\varepsilon - \varepsilon_c)^{0.19}}$ Where $\varepsilon_c$ is the percolation threshold
Boving and Grathwohl, 2001	$\tau = \varepsilon^{-1/2}$

(cont. on next page)

**Table 2.1. (cont.)**

<p>Yu and Li, 2004</p>	 $\tau = \sqrt{1-\varepsilon} \frac{\sqrt{\left(\frac{1}{1-\varepsilon}-1\right)^2 + \frac{1}{4}}}{1-\sqrt{1-\varepsilon}}$
	 $\tau = 1 + \frac{1}{2} \sqrt{1-\varepsilon}$
	$\tau = \frac{1}{2} \left[ 1 + \frac{1}{2} \sqrt{1-\varepsilon} + \sqrt{1-\varepsilon} \frac{\sqrt{\left(\frac{1}{1-\varepsilon}-1\right)^2 + \frac{1}{4}}}{1-\sqrt{1-\varepsilon}} \right]$
<p>Matyka et al., 2008</p>	$\tau = 1 - 0.77 \ln(\varepsilon)$
<p>Khabbazi et al., 2016</p>	$\tau = a - b \ln(\varepsilon)$ <p>Aspect ratio=1 → a=1.01, b=0.37  Aspect ratio =2 → a=0.99, b=0.80  Aspect ratio =3 → a=0.98, b=1.16</p>

Chen et al. investigated the effect of pore geometry on the transport properties by using fractal model. Their results were obtained based on the analytical and numerical simulations which proved that permeability values that are calculated via KC relation gives considerably different results from the simulation results. This difference exhibits the requirement of the consideration of the pore structure. Because KC relation considers only porosity, it was observed that using this equation for fractal geometries gives inaccurate results for permeability (Chen et al., 2015). Xiao et al. conducted a study in order to obtain relative permeability values of liquid flow through unsaturated porous media. By using Monte Carlo model, they have tried to derive a model which defines permeability as a function of capillary pressure and tortuosity of capillaries. The dependency between phase fractal dimensions and porosity was executed. Their proposed model was found to be applicable for various applications in porous media, due to the good agreement observed between the validation results (Xiao et al., 2012). In another

study conducted with nanofibers by Xiao et al., permeability values were found as in an explicit relation with the fractal dimensions of nanofiber structures and the porosity (Xiao et al., 2016). Similarly, Yang et al. derived an equation of permeability specifically for roughened porous media containing a bundle of tortuous capillaries. During their studies, they tried to investigate the effects of tortuosity, fractal dimensions, and relative roughness on permeability. The derived equation showed that, as the relative roughness increases, permeability diminishes. Also, in terms of the roughness effect, the permeability values of roughened surface were found higher than the permeability of smooth capillaries with a fourth power of  $(1-\varepsilon)$  value (Yang et al. 2015). In another study, it was shown that KC equation underestimates the permeability results for low porosity values, and therefore a new model is needed to find permeability values. Low values of porosity do exist in several applications considering the transport behavior in porous medium as Woudberg and Du Plessis indicated in their study conducted with the granular and foamlike porous media (Woudberg and Du Plessis, 2008). This condition results in the requirement of a correction to Kozeny-Carman equation for low porosity values which might be seen in the reservoir rocks as focused in the investigated case by Mavko and Nur, with the help of existing porosity values which was encountered in the structure of clean rocks. KC equation was re-examined by the third power of porosity including percolation effect, resulted in more accurate permeability values (Mavko and Nur, 1997). Aside from the practical complicated porous structures, Parada and his colleagues performed a study at a simpler porous media geometry using volume average methods via simulation software for their calculations. They claimed that, KC equation cannot come up with a universal description of permeability, as a function of simple porous media parameters, such as porosity and structure, and pointed out the necessity of taking complex microstructure effects in consideration rather than using KC equation alone, in order to obtain more accurate permeability predictions (Parada et al., 2009). Henderson and co-workers exhibited a generalized form of KC equation that is dependent on three parameters obtained from fitting experimental data for the fractal porous geometries (Henderson et al., 2010). With a more realistic approach by mimicking the natural porous geometries, fractal pore space geometry was investigated by Costa, and he derived a new form of KC equation. It has been proven with the previous results belonging to non-granular systems, the derived equation can be practically used for vesicular rocks or fiber mat systems (Costa, 2006). Select examples of the models derived based on KC relation which belong to the aforementioned studies are tabulated in Table 2.2.



Table 2.2. Relations derived between permeability and porosity

Mavko and Nur, 1997	$K \approx 15(\varepsilon - 0.035)^3 d^2$ D is pore size
Woudberg and Du Plessis, 2008	$K = \frac{d_g^2 (1 - (1 - \varepsilon)^{1/3}) (1 - (1 - \varepsilon)^{2/3})^2}{41.25 (1 - \varepsilon)^{4/3}}$
Henderson et al., 2010	$\sqrt{\frac{K}{\varepsilon}} = \xi \frac{\varepsilon^{(\zeta+2)/2}}{(1 - \varepsilon)^\eta}$ $\xi, \zeta, \eta$ are the material dependent fitting experimental data
Yang et al., 2015	$K = \frac{\pi L_0^{1-D_T} D_f \lambda_{\max}^{3+D_T}}{128 A (3 + D_T - D_f)} (1 - \varepsilon)^4$ $D_T$ and $D_f$ are fractal dimensions $L_0, A$ , and $\lambda_{\max}$ are the structural parameters
Xiao et al., 2016	$\frac{K}{d_f^2} = C_f \frac{\varepsilon^3}{(1 - \varepsilon)^3 [1 + 0.4 \ln(1 / \varepsilon)]}$ $D_f$ is fractal dimension and $C_f$ is porosity dependent constant

Recently, researchers have mostly concentrated on defining an accurate Kozeny Carman constant ( $C_{KC}$ ) which gathers the effects of flow path, shape of the particles and their connections together. In KC relation, this mentioned constant was simply stated as 5 (Kozeny, 1927; Carman 1937;1939). It was indicated that value of  $C_{KC}$  possesses a different value other than 5 for the porous medium different than packed bed spheres, specifically for structures between the dendrites of some specific substances. Further evaluation of permeability by using KC equation with the value of  $C_{KC}$  as 1 gives accurate results (Brown et al., 2002). For the disordered array of spheres, KC constant was calculated as 2.79, 3.62, and 3.80, for the corresponding sphere radius of 2.5, 3.5, and 4.5, respectively, and the permeability results were acceptable in accordance with the validation between experimental studies (Heijs and Lowe, 1995). Different than similar calculation results in literature, KC parameter was calculated as between 8 and 18, for porosities is in the range of 0.45 and 0.8 for fibrous materials. These large values of  $C_{KC}$  were related with the non-uniformity of the porous medium (Chen and Papathanasiou). For the porous media which have staggered arrangements,  $C_{KC}$  was evaluated as 130,

specifically for a porosity of 0.44, and porosity values between 0.4 and 0.88, the inverse relationship between porosity and  $C_{KC}$  was observed (Gamrat et al., 2007).

However, as the flow geometry becomes complex, taking Kozeny Carman parameter as a constant value may lead to erroneous results. Xu and Yu submitted an extended literature review about the various definitions of  $C_{KC}$  and permeability calculations. Specifically, they derived a new equation in order to calculate KC constant which is dependent on the fractal geometry, maximum pore size and the porosity (Xu and Yu, 2008). For natural fibers, Rodriguez et al. re-examined KC equation with empirically measured permeability values, and according to their conclusion, regardless of the KC constant; the empirical coefficients have changed with the specific material type, and the data did not fit well in KC equation (Rodriguez et al., 2004). Khabbazi and Bazylak derived expressions for two different geometries including arrays of infinite cylinders and spheres in order to obtain more accurate KC relation parameters. The results procured via LBM showed that using functional expressions of Kozeny Carman parameter by taking porosity into account, instead of taking this parameter as a constant value yields more accurate permeability result (Khabbazi et al., 2013). Ozgumus and her colleagues proposed a relationship between Kozeny-Carman constant and porosity by taking pore-to-throat size into consideration. They have proven that for a constant porosity and hydraulic diameter value, permeability differs due to the discrepancies between pore to throat sizes. This conclusion implies the necessity of considering pore to throat size ratio when Kozeny Carman equation is used. Results obtained by using suggested equation were in good accuracy in terms of estimating permeability values (Ozgumus et al., 2014). Xiao et al. reported a function for permeability, and KC Constant for the fibrous materials with the help analytical solution obtained via fractal model. They indicated that the value of Kozeny Carman Constant should vary with geometry of porous medium. Moreover, their results also show that for the porosities higher than 0.8, this constant has the value of 18. (Xiao et al., 2016) Some of the suggested correlations mentioned above can be found in Table 2.3.

Table 2.3. The suggested relations for determination of Kozeny Carman constant

<p>Xu and Yu, 2008</p>	$C_{KC} = \frac{1}{36C_f} \frac{\varepsilon^{(3-D_T)/2}}{(1-\varepsilon)^{(1-D_T)/2}}$ <p><math>D_T</math> is fractal dimension  <math>C_f</math> is the coefficient dependent on <math>D_T</math></p>
<p>Khabbazi et al., 2013</p>	$C_{KC} = 5420 \varepsilon - 5.6 ^{0.6} + 3.38$ <p>Staggered parallel fibers</p>
<p>Ozgumus et al., 2014</p>	$C_{KC} = 9.63\varepsilon + 0.02$ <p>BCC array of spheres</p>
<p>Xiao et al., 2016</p>	$C_{KC} = A\varepsilon^B$ $A = C_0R_{pt}^4 + C_1R_{pt}^3 + C_2R_{pt}^2 + C_3R_{pt} + C_4$ $B = D_0R_{pt}^4 + D_1R_{pt}^3 + D_2R_{pt}^2 + D_3R_{pt} + D_4$ <p><math>\alpha</math> is a function of fractal dimensions</p>

### 2.3. Effect of Throat Size on Permeability

Evaluation of permeability, solely by looking at the porosity itself could be misleading; for instance, the study of Bahga et al. offer an example of a highly porous structure with nearly non-existing permeability values. They based the explanation on the interconnectivity issues of the material; although a highly porous structure is present, the lack of interconnections between the pores has not allowed a flow through the pores (Bahga, 2016). Basically, if the pore throat structures are highly tight, then flowing of the fluid through the throats becomes nearly impossible due to the surface tension forces (Serra, 1984). In such cases, estimation of permeability by measuring porosity does not always present decent results, and to prevent any incorrect permeability predictions, pore throat size should also be considered together with porosity.

Micro/nanoscale porous media have rather complicated and tight porous structures. Particularly, for the unconventional reservoirs whose large pore dimensions and relatively small throat sizes make them different from the conventional ones, the ratio between pore and throat sizes is investigated in detail by several researchers, and some attempts have been done for defining pore-to-throat size ratio as a function of porosity.

Sui and Xian proposed a model with the parameters which have physical explanations in order to investigate water resistance ability of rocks by measuring pressure drop for the granular porous media. In their model, pressure drop was defined as a function of both porosity, tortuosity, and pore-to-throat size ratio, and pore-to-throat size ratio ( $R_{pt}$ ) is defined in terms of porosity (Eq. 2.2). They validated the proposed model with the results obtained by using Ergun equation with the experimentally measured parameters (Sui and Xian, 2009).

$$R_{pt} = \frac{1}{1 - \sqrt{1 - \varepsilon}} \quad (2.2)$$

In their experimental work, Glover and Déry measured the pore and throat sizes for glass bead packs, specifically to observe how streaming potential affected by those geometrical aspects. They showed that pore-to-throat size ratio can be defined as a linear function of porosity with a coefficient of 1.66 (Eq. 2.3) which is valid for randomly distributed monodisperse solids (Glover and Déry, 2010).

$$R_{pt} = 1.66\varepsilon + 1 \quad (2.3)$$

Jin and his colleagues conducted a study for the investigation of water flow in pore-throat nanochannels by using LBM. They indicated that, permeability decreases as the pore-to-throat size ratio increases, such that, for a constant pore diameter relative change in permeability nearly increase by 4-fold, as pore-to-throat size ratio increased from 1 to 4. Thus, the effect of pore to throat size ratio should not be ignored for the permeability predictions (Jin et al., 2016). Zhang and co-workers investigated the effect of pore-throat size on permeability for tight sandstone reservoirs by measuring the pore and throat sizes with  $N_2$  adsorption method. The measured results yielded to pore-to-throat size ratio which was between 50 and 500. By that, they included the shape and size effect on the permeability analysis quantitatively. (Zhang et al., 2016). Gao and his colleagues experimentally measured pore and throat sizes of tight oil reservoirs via rate mercury intrusion porosimetry, and the mean pore-to-throat size ratio was reached between 86 and 503, due to the characteristic of the tight reservoirs which have extremely low throat sizes in comparison to the pore size. The strong relation between pore-to-throat size ratio and fluid displacement efficiency is indicated, and for the large values of pore-to-throat-size ratio, significant reduction in oil recovery can be concluded (Gao et al.,

2016). Dianshi et al., on the other hand measured the pore-to-throat size ratio in the range of 7.5-64 by using the rate controlled porosimetry and nuclear magnetic resonance technique for the tight sandstone (Dianshi et al., 2016). In order to find the clay content in tight sandstones, another experimental study was realized by Cao and co-workers using Mercury injection capillary pressure (MICP) and N<sub>2</sub> gas adsorption method which yields pore-to-throat size ratio results between 2 and 10 (Cao et al., 2016).

For flow resistance through porous media, Wu and Yu suggested a new model depending on the fractal properties of porous medium. Their suggested model is primarily dependent on the pore-to-throat size ratio, fluid characteristics, and the dimensions of pore and particles. They validated the resulting model with the experimental results (Wu and Yu, 2007). Following this, the proposed fractal model associated with the Ergun model was used to analyze flow characteristics in mine water inrush which was affected from rock porosity, form of the particle, fractal and particle dimensions, and pore to throat size ratio. They concluded that the Wu-fractal model plays a major role on mine water inrush in comparison to Ergun equation (Wu et al., 2014).

## **2.4. Permeability of Small Scale Porous Medium**

For the macroscopic flow, bulk fluid has a major role on the identification of flow characteristics, and the surface effects can be considered negligible. However, as the size of the flow domain diminishes, the layer near the surface becomes considerable, and flow behavior diverges from continuum. For those types of flows, conventional no-slip boundary conditions are not applicable any more. As it was summarized in Section 2.1, flow through small scale porous media is a promising topic due to its vast application improving based on nanotechnology.

Due to vast usage of the nanomembranes in several applications, the flow characteristics need to be understood for improvements in related areas. Majumder et al. have proved that flow in the Carbon Nano Tube (CNT) membranes is significantly faster than what might be predicted by conventional theories, including four to five orders of magnitude. Their results explain that the nearly frictionless flow observed at fluid-surface interface of CNT. It was also observed that, initial permeability of the flow decreases with the decrease in slip length (Majumder et al., 2005; 2011). Holt et al., showed the effect of

surface of CNT walls on the permeability values for both water and air, by considering slip flow (Holt et al., 2006).

An attempt to include slip flow effects on permeability calculations was made by several researchers who specifically concentrated on petrological studies. Javadpour and his colleagues measured slip length at a  $50 \times 50 \mu\text{m}$  sample with Atomic Force Microscopy (AFM), and they calculated an apparent liquid permeability as a function of viscosity and friction, that was evaluated by stochastic method. Their results showed that slip corrected permeability was significantly higher than the intrinsic permeability; hence, it was concluded that those slip effects could be the reason of the fluid loss which occurs during the hydraulic fracturing (Javadpour et al., 2015). A similar apparent liquid permeability derivation has been performed by Appiah et al., and it was shown that the discrepancy between the resulting values of apparent liquid permeability and Darcy's permeability increases as the pore diameter decreases, and apparent liquid permeability value increases as slip length increases (Appiah et al., 2013). More recently, a mathematical model for the determination of liquid permeability of oil flow through organic nanopores has been constructed with the help of molecular dynamics simulations. The results showed that slip effect may be ignored for systems that have pore radii greater than 200 nm (Cui et al., 2017). Effects of liquid slip in nanopore and pore geometry have been investigated by Afsharpoor and Javadpour by the aid of CFD simulations. Primarily, they have studied channel flow with different cross sections, followed by porous media with a pore network model. Their apparent permeability results showed that, as the velocity slip increases, deviations on results were found to be growing, based on geometrical effects. Also, involvement of slip effect in the model used for permeability prediction results in permeability values that are significantly different from the ones that have been calculated via Darcy's equation. Furthermore, this discrepancy between results increases as the pore diameter decreases (Afsharpoor and Javadpour, 2016).

## **2.5. Micro/Nanoscale Liquid Transport**

Small scale porous media has been widely investigated in several areas specifically including petroleum engineering, micro/nano membranes, and Lab-on-a-chip devices as discussed previously. Decrease in the flow area makes the continuum assumption non-applicable. Hence, in order to understand liquid transport behavior in

micro/nanoscale porous medium, non-equilibrium between liquid and solid surface should be comprehended. In this sub-section, a brief literature survey about velocity slip for liquid transport, and particularly, non-equilibrium surface conditions in terms of wettability are exhibited.

### 2.5.1. Slip velocity and Slip Length

Liquid velocity at a boundary presents various conditions among slip, no-slip and even stick of multiple molecular layers (Koumoutsakos, 2003). While the velocity stick is mostly effective for channels smaller than ten molecular diameter sizes (Xu and Li, 2007) and, is considered as no-slip for the remaining scales. No-slip condition is common for superhydrophilic and rough surfaces. But, many recent technologies employ atomistically smooth boundaries where strong slip develops. The idea about the velocity slip was first proposed by Navier (1823). According to the Navier's well known boundary conditions, the velocity at the surface  $v_{slip}$ , is proportional to shear stress at the wall (Gad el Hak, 1999).

$$v_{slip} = L_s \left. \frac{dv}{dy} \right|_{@wall} \quad 2.4$$

where  $\left. \frac{dv}{dy} \right|_{@wall}$  is the velocity gradient at the wall, and  $L_s$  is the slip length. Slip length measures the velocity slip as a fictitious distance at which the velocity extrapolates to the value of zero. Slip length is expected to depend on properties of solid and liquid couples as well as on the flow dynamics. In literature, research has been focused on the effects of interfacial properties (Jabbarzadeh et al., 1998; Barratt and Bocquet, 1999; Bizome et al., 2002; Koumoutsakos et al., 2003; Cho et al., 2004; Schmatko et al., 2005; Voronov et al., 2006,2007; Huang et al., 2007,2008; Sendner et al., 2009; Sun et al., 2012; Sofos et al., 2013; Zhang and Chen, 2014; Yen, 2015; Yen and Soong, 2016; Alvarado et al., 2016), shear rate (Jabbarzadeh et al., 1998; Craig et al., 2001; Choi et al., 2003; Joseph and Tabelling, 2005; Li et al., 2014), and channel height (Cheng and Giordano, 2002; Lichter et al., 2007; Xu and Li, 2007; Lee et al., 2012) on slip length. The extensive literature survey shows that studies about the dependence of slip length on the surface and flow properties are widespread, and there is a consensus about the direct relation between slip length, liquid/solid interaction energies and shear rate.

Conversely,  $L_s$  and channel height dependency is not as clear as the conclusions about the dependency on most of the other parameters. For example, some researchers claim that slip length is independent of the channel height. Cheng and Giordano developed this conclusion for Poiseuille's flow experiments at scales between  $2.7 \mu\text{m}$  to  $40 \mu\text{m}$  (Cheng and Giordano, 2002). Similarly, Bizonne *et al.* concluded that there is no relation between slip and the scale of the flow domain in the range of 1 to several hundreds of nanometers (Bizonne et al, 2005). Recently, Ghorbanian and Beskok presented the variation of slip length by surface properties while it remained constant for a certain liquid/solid couple at any size of confinement (Ghorbanian and Beskok, 2016), For such a case, the ratio of the constant slip length of a given liquid/surface couple with the corresponding flow height can provide a prediction of slip effects onto liquid flow inside different size conduits. Also, known as slip coefficient ( $\beta$ ), the slip length non-dimensionalized with channel height can be utilized to calculate micro/nanoscale effects into the NS solution as a function of confinement's size. While the slip length remains constant, an increase of channel height decreases the slip effects and flow conditions approaches to no-slip continuum solution. Thus, the contribution of velocity slip to liquid transport can be characterized by slip coefficient calculated at the conduit size.

On the other hand, there are also studies presenting variation of slip length per the change of the confinement size (Lichter et al, 2007). Multiple studies on water flow in carbon nano tube (CNT) showed that an increase in CNT diameter decreases the slip length gradually (Thomas et al., 2010; Suk and Aluru, 2013; Yasuoka et al., 2015). In that case, the NS solution was complicated since the normalized NS solution based on dynamic similarity is impossible. Instead, any slip coefficient required for the NS solution of a certain confinement height should be calculated based on the slip length of the corresponding size. In this case, models developed for the variation of slip length with the channel height (Yang and Zheng, 2010) can be useful for NS based theoretical solutions. For example, one can utilize the models developed by Suk and Aluru as  $L_s=0.205+0.1517/R$  (nm) (Suk and Aluru, 2013), or by Thomas et al. as  $L_s=30+44/R^3$  (nm) (Thomas et al., 2010) where  $R$  is the nanotube radius. While presenting an exponential increase in slip length with increase of channel height at very small scales, these studies also show that the slip length converges to a constant value and becomes independent to channel height for confinement sizes bigger than  $\sim 10$  nm. Hence, the idea of using slip coefficient to incorporate slip effects as a function of conduit size can be valid for channels as small as 10 nm.



In summary, numerous reported slip lengths for different liquid/solid couples at various conditions exist. Despite the existing attempts to develop a theoretical slip model for liquid flows, there is no generally accepted conclusion. At this point, our preliminary target is to determine a physical range of slip length and slip coefficient from existing systems studied in literature. A diverse amount of studies on direct or indirect measurements of slip length are summarized in al., 2005).

Table 2.4 which presents the measured slip length values, corresponding characteristic lengths of conduits and resulted slip coefficients. Slip lengths as high as 400  $\mu\text{m}$  (Lee and Kim, 2009) can be observed from the tabulated results. Assuming that the slip length is only defined by surface/liquid couple and remains constant, the slip coefficient value could be negligible in a ten-meter tube while a ten-nanometer tube will create a slip coefficient on the order of  $10^4$ . In addition to this perspective, it was attempted to determine the highest value for a slip coefficient directly from published values. Similar slip coefficient ranges as high as  $10^4$  were observed (Majumder et al., 2005).

Table 2.4. Summary of the slip lengths and the slip coefficient ( $\beta$ ) based on corresponding conduit sizes from the literature.

Reference	Channel Height (nm)	Tube Diameter (nm)	Slip Length (nm)	$\beta$	Solid/Liquid Material
Tretheway and Meinhart, 2002	$3 \times 10^4$		1000	0.033	OTS/ DI Water
Choi et al., 2003	$10^3 - 2 \times 10^3$		30	0.03-0.015	OTS/ DI Water
Koumoutsakos et al. 2003		4.72-4.50	63-31	13.34-6.88	Graphite/ Water
Ou et al., 2004	$127 \times 10^3$		$10^3 - 21 \times 10^3$	0.008-0.16	Silicon/ Water
Kassinis, 2004		5.424	18	3.31	CNT/ Water
		2.712	10	3.68	
		4.068	12	3.44	
Majumder et al., 2005		7	$39 \times 10^3$	5571	MWCNT/ Water
			$68 \times 10^3$	9714	
Chun and Lee, 2005	$10^6$		$6 \times 10^3 - 8 \times 10^3$	$6 \times 10^{-3} - 8 \times 10^{-3}$	PDMS/ Water
Joseph and Tabelling, 2005	$10^5$		<100	< $10^{-3}$	PDMS/ DI Water
Cao et al., 2006	10.2		7.9	0.77	Platinum/ Argon

(cont. on next page)

**Table 2.4. (cont.)**

Holt et al., 2006		15	5.1	0.34	Polycarbonate/ Water
		1.6	140- 1400	87.5-875	DWNT/ Water
Cao et al., 2006	10.2		7.9	0.77	Platinum/ Argon
Choi et al., 2006	$3 \times 10^3$		100-200	0.033- 0.066	Silicon/Water
Huang and Breuer, 2007	$5 \times 10^4$		100	$2 \times 10^{-3}$	PDMS/ DI Water
Lichter et al., 2007	0.14		0.44	3.14	FCC Surface/ n-decane
	1.4		1.96	1.4	
Byun et al., 2008	$2 \times 10^5$		$2 \times 10^3$	0.01	PDMS/ Water
Thomas and McGaughey, 2008		1.66-4.99	30	18.07- 6.01	Graphene/ Water
Martini et al., 2008	3		2-22.0	0.17-1.83	FCC Representative Surface/ n-decane
Whitby et al., 2008		44	26-35	0.6-0.8	CNT/ Water
Thomas et al., 2010		1.5-5	115-30	6-76.6	Graphene/ Water
Falk et al., 2010		1	500	500	CNT/ Water
		7	120	17.14	
Qin et al., 2011		0.81	53	65.43	CNT/ Water
		1.59	8	5.03	
Majumder et al., 2011		$34 \times 10^3$ - $126 \times 10^3$	53.3	$1.56 \times 10^{-3}$ - $4.23 \times 10^{-4}$	CNT/ Water
Groombridge et al., 2011		3	1.325- 1.231	0.44-0.41	CNT/ Water
		4	1.069- 1.151	0.27-0.29	
		6	1.018- 1.097	0.17-0.18	
		9	1.087- 1.072	0.12	
		12	1.207- 1.222	0.1-0.102	
Roy et al., 2013	$30-2 \times 10^5$		0- $10^3$	0.005- 33.3	FCC Representative Surface/ Water
Li et al., 2014	100		3.66	0.01	Silicon/ DI Water
Rogers and Wirth, 2012	15-800		63	4.2-0.078	Silica Colloidal Crystals/ Water

\*OTS: Octadecyltrichlorosilane, DI: Deionized, MWCNT: Multiwalled CNT, DWNT: Double walled CNT, PDMS: Polydimethylsiloxane

## 2.5.2. Effect of Wettability

Overall, the micro/nano-scale non-equilibrium liquid dynamics can be taken into consideration using velocity slip in NS solution for confinement bigger than certain sizes (~50 nm). However, velocity slip values cannot simply be calculated by any theory; instead these conditions should be measured either by experiments or molecular simulations specifically for corresponding liquid/solid couples; but this is very challenging and perhaps, unfeasible. On the other hand, as the momentum and thermal exchange coupling between liquid and solid is a direct function of interfacial energy, slip and jump conditions can be expressed by surface wetting phenomena and may be simply predicted by contact angle ( $\theta$ ) measurements.

The angle at a liquid–vapor–solid interface is known as the contact angle and can be utilized to qualitatively measure surface wetting. When a drop of liquid is on a solid surface, it may remain as a spherical drop or spread to cover the solid surface. Specifically, wetting occurs when the contact angle is less than  $90^\circ$ , while the liquid does not wet the surface for contact angle values greater than  $90^\circ$ . For such a case, water/solid interactions are classified as hydrophilic if the contact angle is less than  $90^\circ$ , hydrophobic if the contact angle is greater than  $90^\circ$  and super-hydrophobic if the contact angle is greater than  $150^\circ$  (Yeh et al., 2009). Frequently, the relationship between the contact angle, liquid surface tension, liquid/solid interfacial energy and solid free surface energy is defined by Young's equation. However, other surface properties exist, in addition to the contact angle and, need to be considered to determine interaction of liquid with solid surface and wetting behavior. For instance, the surface morphology, also called roughness, is one of the major properties to determine wetting. Wetting of a rough surface can be homogeneous if the liquid fills in the surface roughness or can be heterogeneous if the liquid stays on top of the surface grooves, which are filled with air. For this reason, measured contact angles cannot be correlated with interface tensions using Young's equation. Instead, Wenzel's model should be employed for homogenous wetting, while the Cassie–Baxter model is applicable for heterogeneous wetting of non-flat or composite/textured surfaces.

Multiple researchers investigated the effect of wettability on velocity slip conditions. Overall, the hydrophilic surfaces were found to develop no-slip and no-jump boundary conditions while the hydrophobicity prevails the slip behavior (Cho et al., 2004;

Majumder et al., 2005; Joseph and Tabelling, 2005; Lauga et al., 2005; Neto et al., 2005; Cao et al., 2006; Joseph et al., 2006; Voronov et al., 2007; Huang et al., 2008; Kou & Bai, 2011; Maali and Bhushan, 2012; Roy et al., 2013; Maynes et al., 2013; Enright et al., 2014). However, correlating slip to wetting is not an easy task. For such a case, Huang et al.'s study is one of the first attempts to model slip and jump conditions in terms of wetting as a function of contact angle (Huang et al., 2008). Their correlation was based on the relationship between slip length and the solid-liquid friction coefficient which was estimated by the force autocorrelation function of the Green-Kubo formulation for the total lateral force acting on the surface. Hence, the fluid-solid interaction was associated to the mean squared interaction force related to the square of fluid/solid interaction energy parameter. Similarly, the Laplace estimate of the interfacial tensions is related to the liquid/solid interaction energy in that combining these in Young's equation portrays the relationship between slip length and contact angle ( $\theta$ ) as,

$$L_s \approx (1 + \cos\theta)^{-2} \quad (2.5)$$

Huang et al. performed an extended MD study to measure both contact angle and slip velocities of surfaces at various interaction strength and conditions. While the results showed very similar behavior with Equation (2.5), Sendner et al. carried this discussion further by critiquing the limits of  $1+\cos\theta$  term and they proposed Equation (2.6) (Sendner et al., 2009).

$$L_s \approx (180^\circ - \theta)^{-2} \quad (2.6)$$

Table 2.5. Summary of slip length measurements with corresponding contact angle values.

Study	Label	Contact Angle (°)	Slip Length (nm)	Solid/Liquid Material
Sendner et al., 2009	S1	48-155	0.49-23.82	Diamond/ water
	S2	81.26-143.91	0.82-9.95	Different roughness levels of carbon/ Water
	S3	77.68-139.42	0.56-7.35	
	S4	58.05-138.45	0.28-6.6	
	S5	91.73-140.88	0.24-4.80	

(cont. on next page)

**Table 2.5. (cont.)**

Yen, 2015	Y1	89.9-150.28	0.52-8.75	Si (100) / Water
	Y2	90.76-150	0.25-3.14	
	Y3	91.5-116.94	0.37-0.43	Graphite/ Water
Y4	91.73-116.84	1.44-1.19		
Alvarado et al., 2016	A1	152-61.65	4.03-0.08	Si (111)/ Water
	A2	147.37-60	1.26-0.022	Si (100)/ Water
Yen and Soong, 2016	YS1	84.108-98.73	0.36-0.14	Si (100)/ Water
	YS2	113.49-96.30	2.25-0.75	Graphite/ Water
	YS3	114.36-107.54	2.44-1.12	
	YS4	101.04-113.83	2.85-1.98	

Equation (2.5) and (2.6) were tested for various liquid solid cases by multiple researchers. Yen and Soong studied the relationship between slip length and contact angle for Si(100) and graphite that their results suggested that Huang's findings were only valid for the Cassie-like state (Yen and Soong, 2016). The interactions of water with Si (100) and Si (111) also studied by Alvarado et al. where results showed a slightly better match with Equation (2.5) than Equation (2.6) while the slip lengths were strongly dependent on the solid surface molecular density and resulted depletion length (Alvarado et al., 2016). Sokhan et al. and Koumoutsakos also identified the dominant effect of solid density on slip length (Sokhan et al., 2001; Koumoutsakos, 2003). Voronov et al. studied the effect of molecular size on the slip length and wettability that slip length was found to increase and contact angle to decrease as the molecular diameter for hydrophobic surfaces increased (Voronov et al., 2006, 2007). Effects of liquid polarity were studied by Cho et al and Equation (2.5) was found valid for non-polar liquids while wettability was not found to play an important role on the slip length variation of polar liquids; instead, dipole moments were dominant on slip behavior (Cho et al., 2004). The range of wetting angle and corresponding slip measurements from literature. are tabulated in Table 2.5 which summarizes the published contact angle and slip length ranges measured on different solid/liquid couples while the Figure 2.1 presents available data points.

Proposed relationships given in Equations (2.5) and (2.6) to all data from a variety of different sources and cases were applied. Even though both models cannot calculate the results of a specific case, the overall behavior between slip length and contact angle can be predicted by these models fairly well. Based on existing data, Equation (2.5) shows a better fit in hydrophilic range ( $\theta \leq 90$ ) and Equation (2.6) explains behavior in hydrophobic region ( $\theta \geq 90$ ) better.

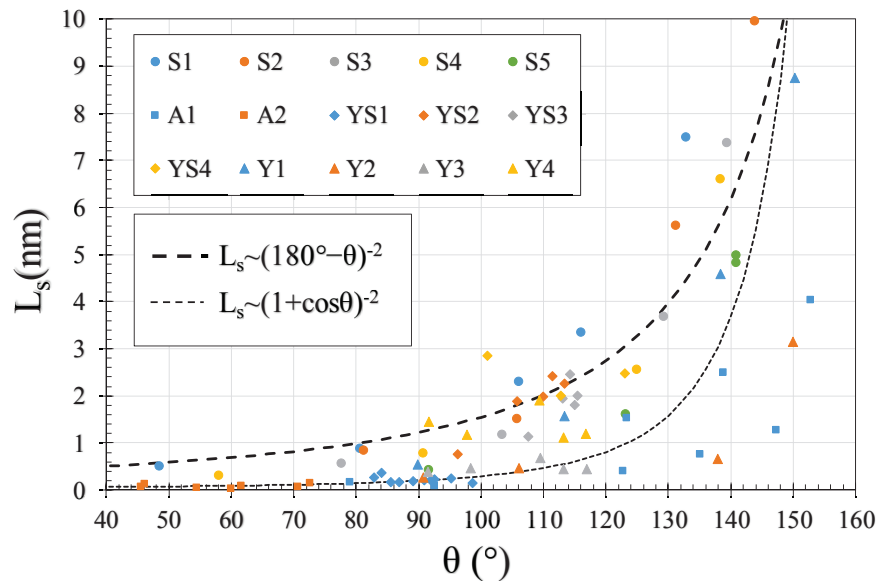


Figure 2.1. Slip length values measured at different wetting conditions.

## CHAPTER 3

### FORMULATION OF THE PROBLEM

#### 3.1. Volume Average Method and Pore Scale Method

Porous media contain solid structures and the voids between these structures where fluid flow occurs. The solid structures can be homogeneously or heterogeneously distributed in the porous medium. Generally, heterogeneous distribution is mostly seen in both natural porous structures and most of the applications. This complex structure of porous media causes difficulties in the characterization of fluid flow through the pores. There are two major approaches to determine the velocity, pressure and temperature distribution of porous medium: microscopic and macroscopic approaches.

In the microscopic approach, continuity, momentum, and energy equations are solved in the voids between solid structures considering three-dimensional flow in the porous medium. With this method, accurate velocity, pressure and temperature distributions are obtained. For a specified porous structure, the continuity and momentum equations for an incompressible, Newtonian fluid flow which has constant thermo-physical properties are written in Equation (3.1) and (3.2)

$$\nabla \cdot \vec{u} = 0 \quad (3.1)$$

$$\rho_f \frac{\partial \vec{u}}{\partial t} + \rho_f (\vec{u} + \nabla \vec{u}) = -\nabla p + \mu_f \nabla^2 \vec{u} \quad (3.2)$$

Where  $\vec{u}$  is the velocity vector,  $p$  is pressure,  $\rho_f$  and  $\mu_f$  are the density and dynamic viscosity of the fluid, respectively. Although this method provides very sensitive results, the applicability of the method, especially for the disordered porous media, is highly difficult and time consuming as well.

As an easier solution method, macroscopic approach is developed by researchers in order to obtain velocity, pressure, and temperature field of studied porous medium. Here, the flow is assumed as one directional, the continuity and momentum equations are solved in the continuum domain rather than pore scale. The continuum domain includes whole

volume without consideration of the interruption on the flow caused by solid structures. The fluid flow in the porous domain is analyzed by conducting volume average techniques.

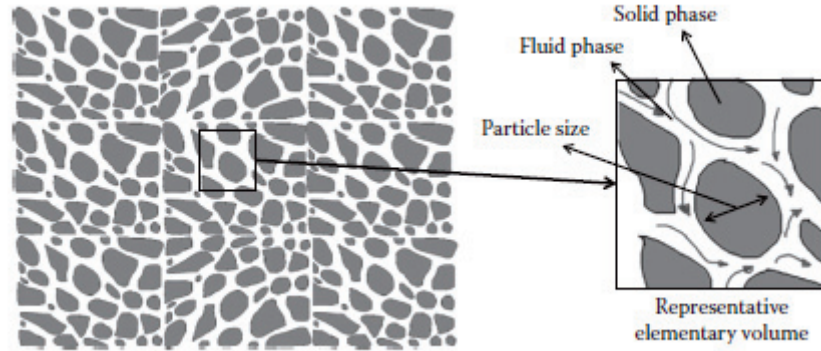


Figure 3.1. Microscopic control volume in a porous structure  
(Source: Mobedi et al., 2015)

Taking volume average of any quantity over a control volume is provided as;

$$\langle \phi \rangle = \frac{1}{V} \int_V \phi dV \quad (3.3)$$

Here,  $V$  denotes the volume of specified control volume. With volume averaging method shown in Equation (3.3), macroscopic velocity is obtained in Equation (3.4).

$$\langle \bar{u} \rangle = \frac{1}{V} \int_V \bar{u} dV \quad (3.4)$$

In order to obtain average value of any one phase, intrinsic averaging can be used. The intrinsic averaging is shown in Equation (3.5), for pore velocity evaluation.

$$\langle \bar{u} \rangle^f = \frac{1}{V_f} \int_{V_f} \bar{u} dV \quad (3.5)$$

Where,  $V_f$  represents pore volume. By that, macroscopic continuity and momentum equations can be obtained by volume averaging as follows;

$$\nabla \cdot \langle \bar{u} \rangle = 0 \quad (3.6)$$



$$\rho_f \left[ \frac{1}{\varepsilon} \frac{\partial \langle \vec{u} \rangle}{\partial t} + \frac{1}{\varepsilon^2} \langle \vec{u} \rangle \cdot \nabla \langle \vec{u} \rangle \right] = \quad (3.7)$$

$$-\nabla \langle p \rangle^f + \frac{\mu_f}{\varepsilon} \nabla^2 \langle \vec{u} \rangle - \frac{\mu_f}{K} \langle \vec{u} \rangle - \frac{C}{K^{1/2}} \rho_f |\langle \vec{u} \rangle| \langle \vec{u} \rangle$$

In the equation above,  $\langle \vec{u} \rangle$  represents local average velocity, and  $\langle p \rangle^f$  denotes intrinsic pressure of the fluid phase flowing through the porous medium. The terms on the left-hand side are the convective inertia terms. Second, third, and fourth terms in the equations identified as Brinkman, Darcy, and Forchheimer terms, respectively (Nakayama, 1995). In the same order, these terms explain boundary friction, porous viscous, and porous inertia in the flow field. In the volume averaged transport equation, there are some additional terms which are not observed in the pore scale governing equations exist. In Equation (3.7), K and C terms are two of those so-called VAM transport parameters, and they are denoted as permeability and Forchheimer coefficients, respectively. For the evaluation of volume-averaged values of pressure and velocity fields, K and C values are required. Since this study was focused on transport of flow with low Re numbers, porous inertia was neglected and hence, Forchheimer coefficient was not used. Another VAM parameter, Darcy motion equation will be explained in the following paragraphs.

### 3.2. Darcy and Kozeny-Carman Equations

Henry Darcy investigated the proportionality between macroscopic velocity and pressure drop as an outcome of his experiment which concentrated on the water filtration through sands. Another observation that Darcy presented is that there is an inverse relation between the macroscopic velocity and fluid viscosity. Basically, this relation became Darcy's Law, and has been used in permeability predictions since its discovery. Darcy's Law can be found in equation (3.8). Here, the proportionality constant K, is called as permeability which is effected from the change in microstructures of solid matrix, whereas it is independent of the fluid properties (Nakayama, 1995). It is important to note that, in order to use Darcy's Law for the evaluation of velocity, first, Re number of the flow should be checked since Darcy's Law is only applicable in low Re region due to non-consideration of the viscous effects.

$$\langle u \rangle = \frac{K}{\mu_f} \left( \frac{d\langle p \rangle^f}{dx} \right) \quad (3.8)$$

Accurate estimation of Darcy velocity is only possible by knowing corresponding permeability values of porous medium, and the most appropriate way to estimate permeability values can be achieved by using Kozeny Carman equations. In addition to the information that has been given in the introduction section, the derivation is going to be explained in the following paragraphs.

Kozeny performed his study for a system which includes several parallel cylinders which flow through in it. Hence, as a starting point, the average velocity for Hagen-Poiseuille flow in a channel with diameter of  $d_t$  can be written as:

$$\langle u \rangle^f = -\frac{1}{32\mu} \frac{d\langle p \rangle^f}{dx} d_t^2 \quad (3.9)$$

Combination of Hagen-Poiseuille flow equation in channel flow with Darcy's Law, permeability value of corresponding flow can be written as follows;

$$K = d_t^2 \varepsilon / 32 \quad (3.10)$$

Additional to these, if the tortuosity concept included into the Equation (3.10), the related equation becomes;

$$K = \frac{d_t^2 \varepsilon}{32 \tau} \quad (3.11)$$

where the term  $\tau$  is tortuosity which can be explained as the ratio between actual path that fluid flows in the porous media and the path where the fluid is thought as flow in the straight domain in the absence of interruptions caused by solid matrix in porous media.

Kozeny's proposed equation which gives permeability results then re-considered by Carman. Next, Kozeny-Carman equation (Equation (3.11)) is identified which has been specifically focused on packed bed of spheres and yields permeability results for specified geometry.

$$K = \frac{d_h^2 \varepsilon}{16 C_{KC}} \quad (3.12)$$

Here,  $d_h$  is the pore hydraulic diameter of the porous medium which can be found as;

$$d_h = \frac{4\varepsilon}{A_0(1-\varepsilon)} \quad (3.13)$$

where  $A_0$  is the ratio of the fluid-solid interfacial area to the solid volume. The term which was denoted as  $C_{KC}$  in equation (3.12) is called as Kozeny Carman Constant which includes the effects of flow path, particle shape and their connections (i.e., tortuosity and shape effects). The value of Kozeny Carman Constants was first proposed as 5. For spherical particles, the Kozeny- Carman equation can be re-considered based on the idea of hydraulic diameter as follows;

$$K = \frac{1}{36C_{KC}} \frac{\varepsilon^3}{(1-\varepsilon)^2} d^2 \quad (3.14)$$

where  $d$  is the diameter of the spheres. The proposed model based on one-dimensional flow can be updated for two or three-dimensional cylinders as it was shown in Equation (3.14).

$$K = \frac{1}{16C_{KC}} \frac{\varepsilon^3}{(1-\varepsilon)^2} d^2 \quad (3.15)$$

where  $d$  is the diameter of the cylinders.

As mentioned before, permeability can be measured experimentally. However, this is both time consuming and costly way to estimate permeability. A more convenient way to predict permeability is using the volume average approach to the microscopic equations.

### **3.3. Governing Equations and Boundary Conditions for Determination of Permeability**

In this study, water is chosen as a Newtonian and incompressible working fluid with constant thermo-physical properties. The flow in the pores is presumed as steady, and laminar with  $Re < 1$  in order to provide the flow in Darcy region. Specifically, the density and viscosity values for water flow was taken as  $1000 \text{ kg/m}^3$ ,  $8.9 \cdot 10^{-4} \text{ Pa.s}$ , respectively. Here, the fluid flowing is assumed as through the square rods and based on this, idea for performing a solution via volume average approach, a representative elementary volume

where the fluid flow is analyzed and illustrated in Figure 3.2. In the enlarged version which specifically represents REV bounded by the dashed lines, the terms D and H indicates pore diameter and the distance between the center of the pores. For this system, the steady form of the continuity and momentum equations are analyzed in order to obtain velocity and pressure field in the pores of considered REV.

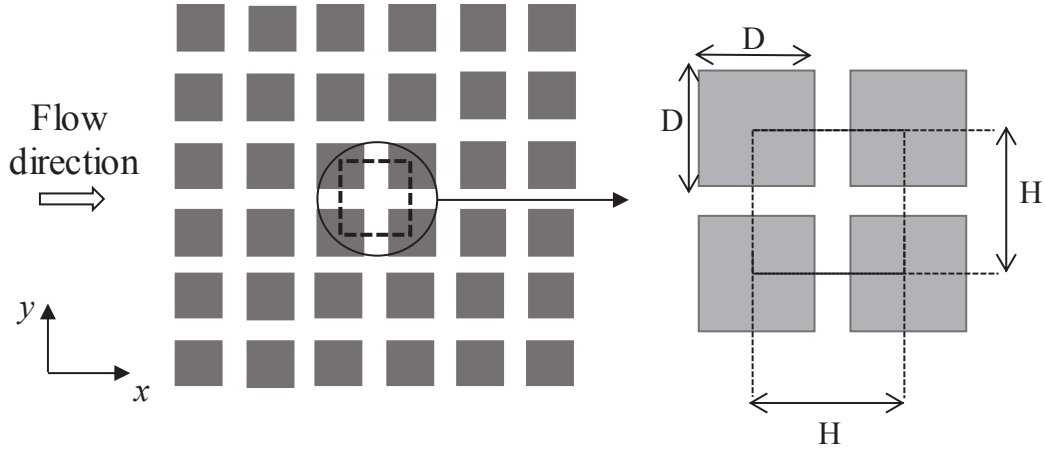


Figure 3.2 Schematic view of the considered porous media, and REV which drawn with the dashed lines (right).

Permeability of considered porous media can be evaluated by investigating the microscopic governing equations. Velocity and pressure distributions in the pores can be obtained via the solution of continuity and momentum equations, respectively. With the assumptions indicated above, the continuity and momentum equations for the flow in the rectangular coordinates can be written as follows;

$$\frac{\partial u}{\partial x} + \frac{\partial v}{\partial y} = 0 \quad (3.16)$$

$$u \frac{\partial u}{\partial x} + v \frac{\partial u}{\partial y} = -\frac{1}{\rho} \frac{\partial p}{\partial x} + \nu \left( \frac{\partial^2 u}{\partial x^2} + \frac{\partial^2 u}{\partial y^2} \right) \quad (3.17)$$

$$u \frac{\partial v}{\partial x} + v \frac{\partial v}{\partial y} = -\frac{1}{\rho} \frac{\partial p}{\partial y} + \nu \left( \frac{\partial^2 v}{\partial x^2} + \frac{\partial^2 v}{\partial y^2} \right) \quad (3.18)$$

In the equations above,  $u$  is the velocity component in  $x$  direction, and  $v$  is the velocity component in the  $y$  direction. Also, the terms of  $p$ ,  $\rho$ , and  $\nu$  denote pressure, density, and kinematic viscosity, respectively.

The flow is taken as unidirectional in the  $x$  direction, due to consideration of the symmetry with respect to  $x, y$  directions, and additionally  $xy$ , and  $yx$  diagonals. In order to obtain permeability values of the considered porous medium, the continuity and

momentum equations are solved with the boundary conditions which are given in the Eqs. (3.19-3.22).

$$\text{On solid walls:} \quad u = u_s = -L_s \frac{\partial u}{\partial y}, \quad v = 0 \quad (3.19)$$

$$\text{For inlet boundary:} \quad u(0, y) = f(y), v(0, y) = 0 \quad (3.20)$$

$$\text{For outlet boundary:} \quad \frac{\partial u(H, y)}{\partial x} = \frac{\partial v(H, y)}{\partial x} = 0 \quad (3.21)$$

$$\text{Symmetrical boundary conditions:} \quad \frac{\partial u}{\partial y} = \frac{\partial v}{\partial y} = 0 \quad (3.22)$$

As a next step, calculations of Darcy velocity and pressure gradient in x direction for the flow in half section of the considered porous medium are shown in below.

$$\langle u_f \rangle = \frac{2}{H^2} \int_0^{H/2} \int_0^H u \, dx \, dy \quad (3.23)$$

$$-\frac{d\langle p \rangle^f}{dx} = \frac{2}{H(H-D)} \left[ \int_{D/2}^{(H-D)/2} p|_{x=0} \, dy - \int_{D/2}^{(H-D)/2} p|_{x=H} \, dy \right] \quad (3.24)$$

For this study, permeability tensor becomes as follows;

$$\begin{pmatrix} \langle u_f \rangle \\ \langle v_f \rangle \end{pmatrix} = \frac{1}{\mu} \begin{pmatrix} K_{f,xx} & 0 \\ 0 & K_{f,yy} \end{pmatrix} \begin{pmatrix} \frac{\partial p}{\partial x} \\ \frac{\partial p}{\partial y} \end{pmatrix} \quad (3.25)$$

It should be noted that, in the current study  $K_{f,xx}$  and  $K_{f,yy}$  have the same value since the solution was performed in the symmetrical porous media.

Darcy Law can also be converted into the non-dimensional form as follows,

$$-\frac{H}{\rho \langle u \rangle^2} \text{Re} \frac{d\langle p \rangle^f}{dx} = \frac{H^2}{K} \quad (3.26)$$

Where Re number can be defined as;

$$\text{Re} = \frac{\rho \langle u \rangle H}{\mu} \quad (3.27)$$

The left-hand side of Eq. (3.26) represents the macroscopic pressure drop, while the right-hand side is the reciprocal of the dimensionless permeability. It is clear that, there is a linear relation between the inverse of the non-dimensional permeability and pressure drop. This is valid for the Darcy region, since the permeability is only affected by the structural properties and flow and fluid characteristics do not have a significant role on the permeability.

## CHAPTER 4

### SOLUTION METHOD

In this chapter, the numerical solution method performed to solve governing equations with related boundary conditions is clarified. The iterative method used for obtaining periodical boundary conditions is explained. Computational steps for obtaining solution of REV is given. At the end of this chapter, numerical computations of the velocity profile and pressure drop values are exhibited with the mesh independency result.

#### 4.1. Numerical Procedure

The solution of continuity and Navier-Stokes equations are obtained via Computational Fluid Dynamics (CFD) simulations that use Finite Element Method. All studies are performed with Reynolds number smaller than 1, in order to study within Darcy region. Numerical computations are carried out iteratively to obtain periodical fluid flow boundary conditions. First of all, constant flow velocity is assumed as the inlet velocity. Governing equations are solved by the aid of this assumption and a velocity profile is obtained at the outlet. Resultant outlet velocity profile of the first computational run is given as the inlet velocity of the second run and computations are performed once more. By using this iterative procedure, a fully developed velocity profile is obtained, when the inlet and outlet velocity profiles are exactly matched and, periodical flow boundary conditions are provided.

#### 4.2. Computational Details

As stated previously, computations were carried out with the periodical flow boundary conditions. In the REV, during the solution of governing equations, Finite Element Method was employed. The number, distribution, and the shape of the computational elements are crucial when using finite element method. Optimum mesh case was selected by performing mesh independency test. Through this search, mesh

density which is a factor that indicates the total number of computational units per computational domain was used. Different mesh densities were selected and the mesh dependency of the results were compared. These results are presented in the next chapter. In order to manage discretization of the momentum equation, the selection for discretization was done as 3<sup>rd</sup> power for velocity, and 2<sup>nd</sup> power of pressure. (Shape function of velocity and pressure fields were selected as 3<sup>rd</sup> and 2<sup>nd</sup> power, respectively.) As a convergence criterion, relative error was fixed as  $10^{-7}$  for the evaluation of flow parameters.

### 4.3. Mesh Independency Tests

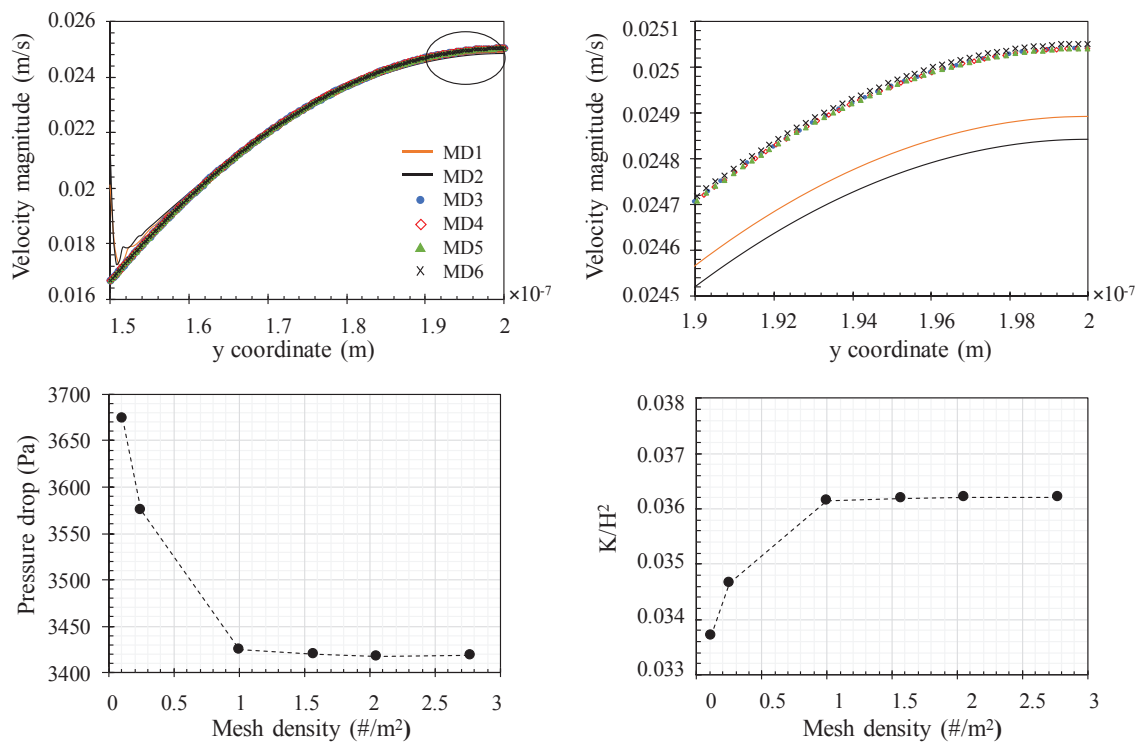


Figure 4.1. Variation of the (a) velocity profile, (b) enlarged view of the velocity profile at the specific location in y direction, (c) evaluated pressure drop values with different mesh densities (d) dimensionless permeability with different mesh densities.

In order to provide mesh independency, the model was computed in several mesh sizes, and the optimum mesh size was selected when the error between consecutive mesh results has converged zero. The mesh size was optimized by considering both the accuracy of the permeability results and minimum CPU usage. Figure 4.1 represents the velocity profile, pressure difference between inlet and outlet conditions, and



dimensionless permeability values that were obtained in different mesh density values where  $\varepsilon=0.4$ ,  $R_{pt}=4$  and  $L_s=50$  nm. As shown in Figure 4.1, there is no longer change between the results of mesh densities of  $2.06 \text{ \#/m}^2$  and  $2.66 \text{ \#/m}^2$ . Hence, the optimal mesh density of  $2.06 \text{ \#/m}^2$  was selected to be used for all computations in this study. Considering the consistency between mesh densities of  $2.06 \text{ \#/m}^2$  and  $1.57 \text{ \#/m}^2$ ,  $1.57 \text{ \#/m}^2$  could have also thought to be used as the optimal size. Nevertheless, pressure distributions have shown obvious fluctuation for mesh density was equal to  $1.57 \text{ \#/m}^2$ . Therefore, by taking these into consideration, the mesh density was chosen to be 2.06 by performing the numerical computations.

## CHAPTER 5

### RESULTS AND DISCUSSION

In this section, the results of permeability calculations at different pore-to-throat size ratios ( $R_{pt}$ ) and at different slip conditions are presented. First, the validation of results is done by comparing them with the published studies. Next, non-continuum effects in the micro/nano pores for the liquid flow is represented in terms slip length and discussed in detail. Finally, the extended form of Kozeny-Carman (KC) relation is proposed as a function of porosity ( $\epsilon$ ), pore-to-throat size ratio ( $R_{pt}$ ) and slip length ( $L_s$ ).

#### 5.1. Calculations of Permeability

For the investigation of the geometrical effects on the transport behavior in the considered porous media, varying pore-to-throat size ratios ( $R_{pt}$ ) are used. At this point, identifying the exact definition of  $R_{pt}$  is required. With this aim, REV is re-drawn with the corresponding size parameters in Figure 5.1. Here, the terms of  $a$  and  $b$  represent the dimensions of the solid particle in  $y$  and  $x$  directions, respectively. If  $R_{pt}$  is identified as the ratio between pore size and the throat size, then the terminological notation becomes as follows;

$$R_{pt} = \frac{\text{Pore size}}{\text{Throat size}} = \frac{H}{H - 2a} \quad (5.1)$$

The sketch located in the right side of the Figure 5.1 shows the computational domain. Due to the symmetrical boundary conditions, all computations are held by taking the half of the REV. It is important to note that, height of the computational domain is taken as 400 nm by considering the possible throat sizes where non-equilibrium behavior can be contributed as a slip boundary conditions.

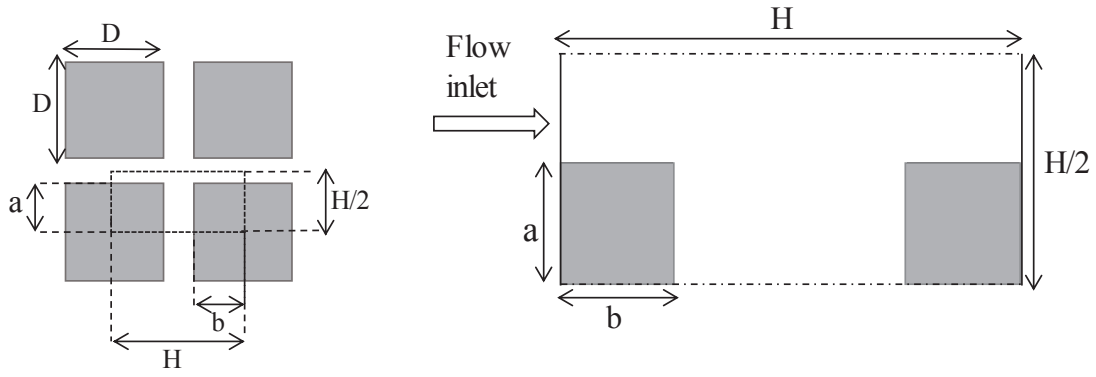


Figure 5.1. Representation of computational domain with geometrical notations.

In order to evaluate velocity of the flow, by using Darcy's Law for permeability calculations, first of all, applicability of Darcy Law should be checked prior to starting the calculation procedure. As it was stated in Darcy's Law, due to the neglect of inertial terms for the small values of Reynolds (Re) number (specifically when  $Re < 1$ ), non-dimensional pressure drop values remain constant. For checking the applicability of Darcy's Law, non-dimensional pressure drop values versus varying Reynolds numbers are drawn for a constant porosity value of 0.4, and the resulting plot was presented in Figure 5.2 in the presence of both slip and no slip flow cases. It was observed that, non-dimensional pressure drop values do not change no matter what value Re number takes between 0 and 3, and with this result, the applicability of Darcy Law is proved. It is important to note that, the applicability of Darcy's Law for small Re number values is already proven by numerous times for the no slip flow cases. However, with the help of this figure it can be shown that, Darcy Law can also be used for the permeability calculation in the slip flow region.

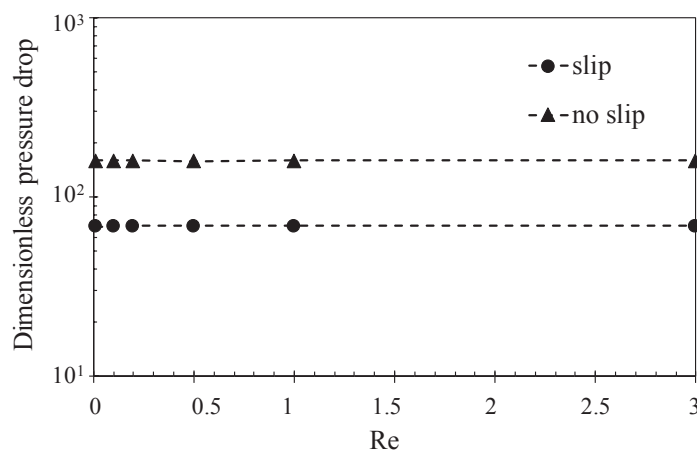


Figure 5.2. The change in the non-dimensional pressure drop values with respect to Reynolds number for both slip and no slip flow cases.

After assuring the applicability of Darcy's Law, the permeability values are calculated as follows. Firstly, for a specified Re number (Eq. 3.27), an inlet velocity value is calculated and this velocity is defined as an inlet velocity value for the first simulation run at CFD software. After solving the governing equations with the corresponding boundary conditions, the outlet velocity is computed by the aid of the computer simulation. The outlet velocity profile of first run is used as the inlet boundary condition for the second run, and problem is solved again. With the help of this iterative procedure, fully developed velocity profile is obtained when the inlet and outlet velocity profiles becomes uniform. When the fully developed velocity profile has been achieved, the velocity, inlet and outlet pressure profiles are extracted. This outlet velocity profile is composed of velocity values that have been computed at each point that have been specified by mesh along the throats. Those velocity values are averaged, and with this mean value of the velocity, Darcy velocity was calculated, using Eq. 3.23. Similarly, the average inlet and outlet pressure values are used to define pressure drop in the specified domain. Finally, permeability values are calculated by using Darcy Law (Eq. 3.8). Validation of the current numerical model is done with the help of existing literature. For different porosities, permeability values are calculated for a REV having pores with a unity aspect ratio which means the squares in the REV with the same dimension (for the case that  $a=b$  in Figure 5.1). Different porosity values varying between 0.1 and 0.9 for a constant aspect ratio is equal to 1 can be observed visually better with the help of Figure 5.3. Then, dimensionless permeability values are obtained by solving the governing equations with no slip boundary conditions in order to make comparison between the results of existing studies performed by Ozgumus et al (Ozgumus et al., 2014) and Saada et al (Saada et al., 2006). The current study was modelled through liquid flow, different than the existing works where gas was used as working fluid. However, using the previous studies to base the validations on would not be wrong since Darcy's law does not specify what kind of fluid should be assigned. As shown in Figure 5.4., outcomes that have been obtained for the present work and results adapted from aforementioned studies are in good agreement.

In addition, results based on the solution with the presence of 50 nm slip length are also represented to show the non-equilibrium effects in terms of slip length on permeability. As shown in Figure 5.4, non-dimensional permeability values in the presence of liquid slip are found to be higher than the ones obtained from no slip flow case. This result is even more prominent for lower porosity values since they possess

more fluid surface interactions which make small scale effects more dominant. This finding will be further discussed in detail with different values of slip length, by the variation of different geometrical parameters such as different values of porosity and  $R_{pt}$ .

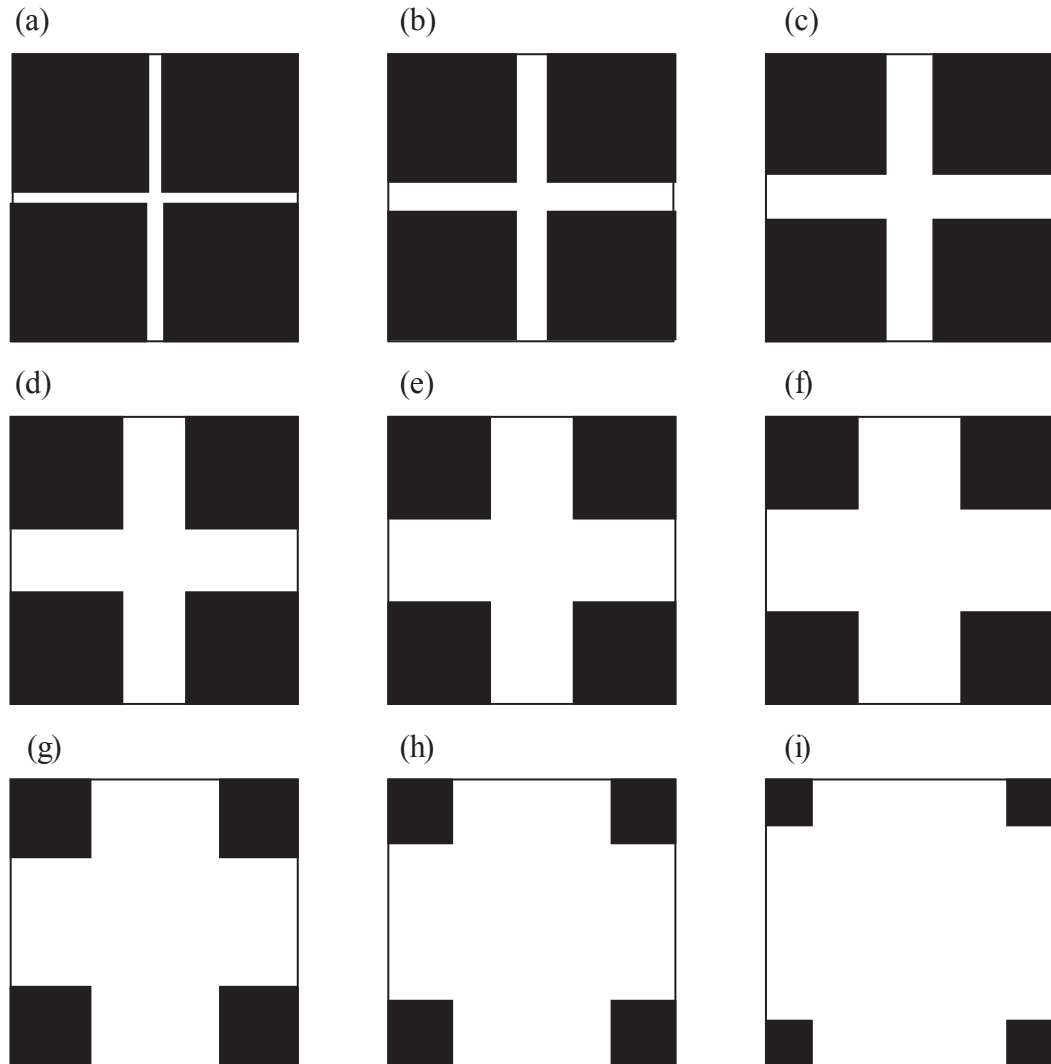


Figure 5.3. Representation of REV when aspect ratio is equal to 1 with different porosities of (a) 0.1, (b) 0.2, (c) 0.3, (d) 0.4, (e) 0.5, (f) 0.6, (g) 0.7, (h) 0.8, and (i) 0.9

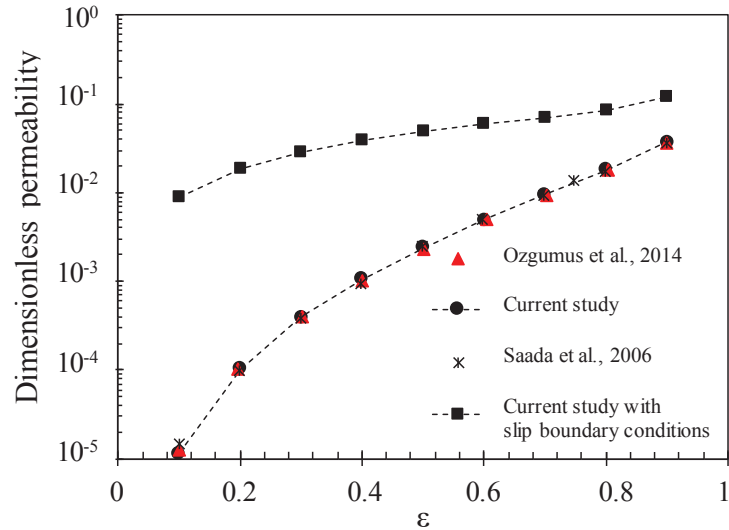


Figure 5.4. Validated results of dimensionless permeability values with reference studies

Characterization of porous media only by taking porosity into consideration is not a completely correct approach and other geometrical effects should be well investigated for the correct predictions of permeability values. Although the relationship between permeability and porosity is well documented, the geometrical effects of porous media have remained almost unstudied. The results exhibited in Figure 5.5 emphasize the importance of the throat size which is one of the major geometrical parameters to be considered. In this study, the effect of throat size is investigated by considering the pore-to-throat size ratio ( $R_{pt}$ ) as a parameter. In Figure 5.5, effects of different  $R_{pt}$  values on the main flow are represented by the aid of the pressure contours and streamlines with the slip effects. Here, the pressure values are normalized with the corresponding inlet pressure distribution for no slip and slip conditions individually. The results that have been gathered for a constant porosity of 0.4, are presented from top to the bottom with respect to three different  $R_{pt}$  values as 10, 6.66, and 3.39. No slip condition, and slip conditions with the slip length ( $L_s$ ) values of 5 nm and 50 nm are represented from left to right. As clearly seen, for a constant porosity value, the behavior of the flow varies in accordance with the change in the  $R_{pt}$ . In the highest  $R_{pt}$  value of 10, the pressure values show a drastic decrease along to pore as the contours exhibit a sudden color change from red to blue, due to the less connectivity between the pores. Whereas, as the  $R_{pt}$  is decreased down to 3.39, the pressure values decrease gradually since the flow domain resembles a channel geometry. Also, as it can be understood by looking at the streamlines, the main flow tends to diverge perpendicularly from the longitudinal direction. Different

connectivity between pores and resultant different values of  $R_{pt}$  yields to secondary flow formation inside pores. Moreover, slip condition also influences the number and patterns of secondary flows, especially for lower  $R_{pt}$  values. For instance, for  $R_{pt}$  of 3.39, no slip and 5 nm slip conditions undergo two pieces of secondary flow patterns, whereas slip length increases to 50nm, the number of secondary flows diminish to 1. As the value of  $R_{pt}$  decreases for both slip and no-slip cases, the fluid tends to flow in more straightforward streamlines, instead of diverging into vertical pore connections, which means the flow in the porous media resembles the flow in the straight channel flow. Additionally, the sudden pressure drops encountered at the corners are more considerable for the small values of  $R_{pt}$ . Although this sudden pressure changes are present at both no slip and slip conditions, it is most observable in highest slip length case. Regarding these results gathered, it can be claimed that, the effect of pore to throat size ratio on flow field is significant, especially for the flow with slip boundary condition. These observations prove that not only porosity, but the changes in the  $R_{pt}$  are also effective for the characterizing the flow in the porous media.

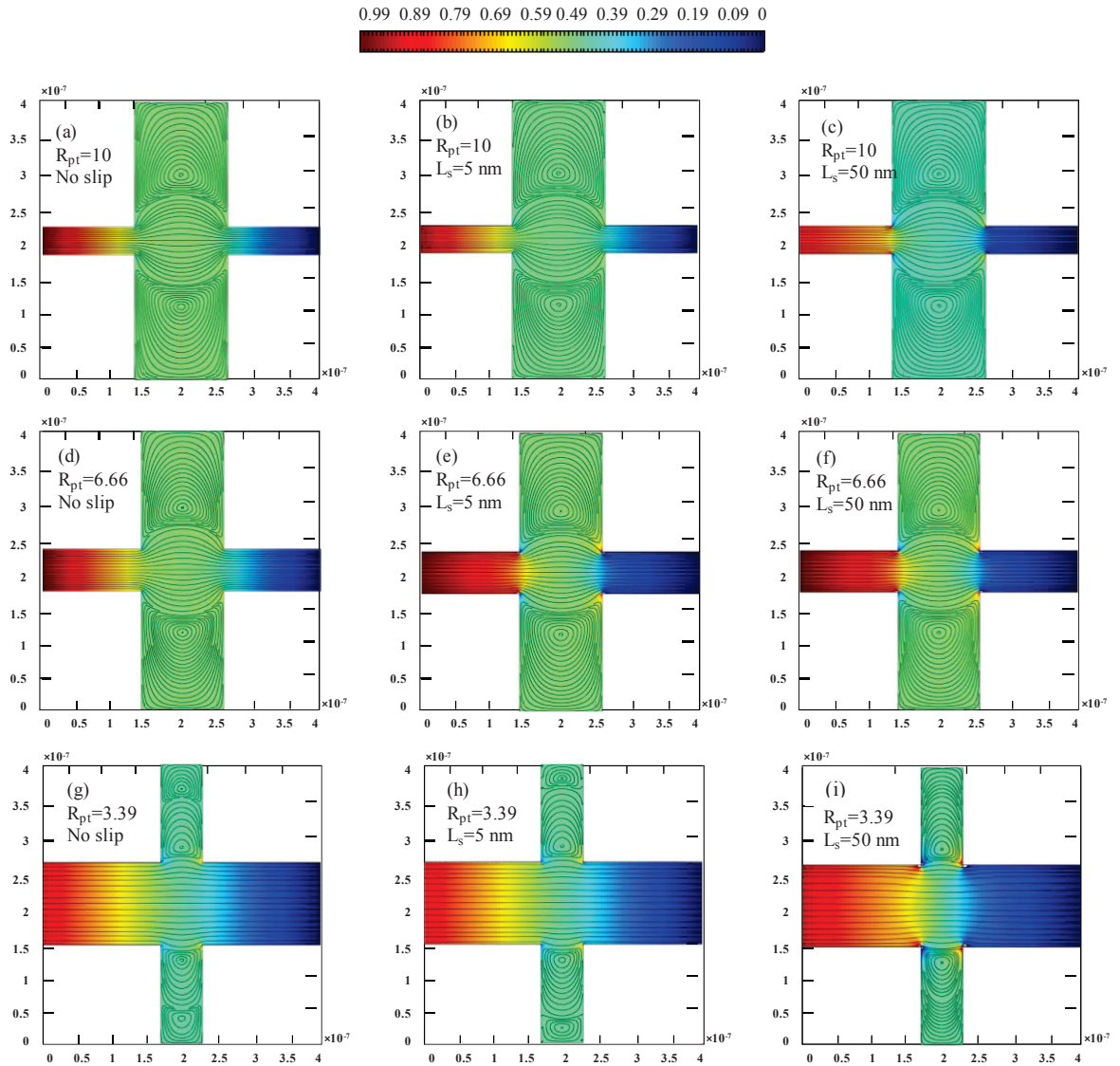


Figure 5.5. Pressure contours and streamlines of REV for a constant porosity of 0.4 and with different  $R_{pt}$  and slip conditions.

For a further investigation of slip effects on the flow, velocity profiles are drawn with different slip lengths and varying  $R_{pt}$  values with the help of velocity contours, and represented in Figure 5.6. Here, the result are obtained for a previously specified porosity values as 0.4, and  $R_{pt}$  values as 10, 6.66, and 3.39. The velocity values are normalized with the mean velocity of each case individually. The mean velocity value is found as very similar for the all cases between (a)-(f). For a better observation of the velocity contours, the velocity contours are drawn in the color scale range of 0 to 1.5 which is the value of  $u_{max}/u_{mean}$  for no slip case in the highest  $R_{pt}$  value. For the no slip condition, velocity gradient through the porous medium gradually becomes linear as the ratio between pore to throat sizes decreases. When this ratio increases, flow velocity in the



longitudinal direction significantly decreases at the throat passages. The non-zero velocity values at the pore surfaces were first examined for the case with 5 nm slip length, then with 50 nm slip length which procures more observable velocity slip in comparison to a lower slip length value. This means that, the increase in slip length from 5 nm to 50 nm yields to a substantial decrease of velocity gradient in the pore surface. Also, specifically for low  $R_{pt}$  values, as the slip length increases, the flow behaves as a plug-like flow, with a more uniform gradient distribution. From a local perspective, the figure helps to explain how the varying slip lengths affect the velocity gradients through the flow domain qualitatively. In the following sections, the results will be quantitatively compared considering the permeability values.

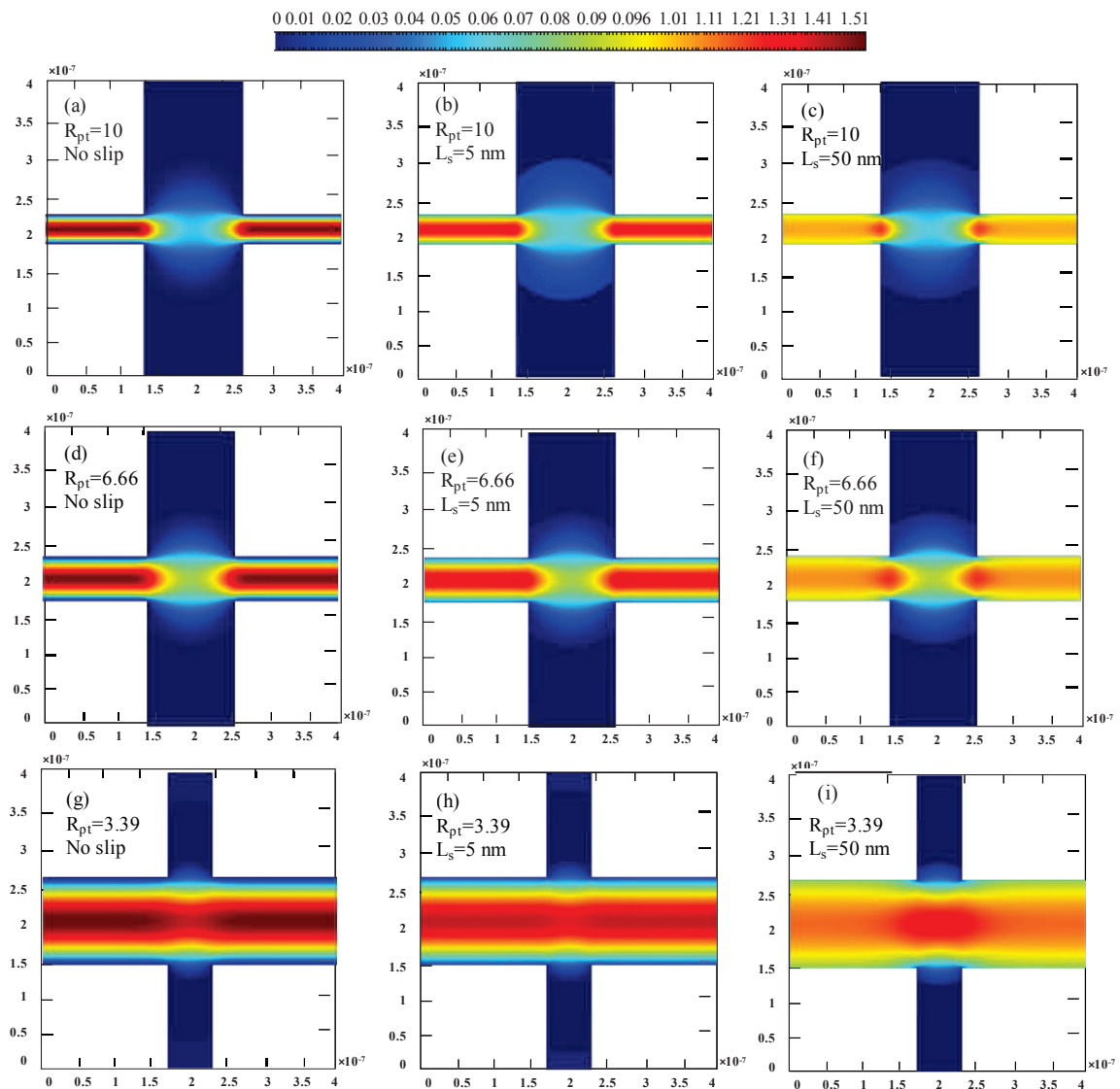


Figure 5.6. Representation of velocity profile with contours by comparing no slip and slip conditions with 5 nm and 50 slip length results for a constant porosity of 0.4 and different values of  $R_{pt}$  and  $L_s$ .

Variations in the flow in pores are represented in Figure 5.7. for a constant  $R_{pt}$  with respect to varying porosities of REV. Here, in order to study with a broad range of porosity, pore to throat size ratio is selected as 4. For the selected pore to throat size ratio, the calculated porosity values of 0.32, 0.4, 0.54, and 0.7 are used and the corresponding results are placed from top to the bottom, respectively. In this figure, how non-equilibrium behavior affects the fluid flow can be revealed by comparing results obtained with no slip and slip boundary conditions. For providing consistency between the range of pressure drop for each case, pressure values are normalized by dividing them to the corresponding inlet pressure values of the specific case. For a given  $R_{pt}$  value, increase in the porosity causes a decrease in the pressure drop in the specified domain. The magnitude of the decrease is found to be considerably high in the no slip case. For no slip, and slip flow with 5nm and 50 nm slip length cases, highest values of pressure drop are observed for the lowest porosity of representative elementary volume as 0.32. Although this conclusion is valid for all cases, as the effect of slip becomes considerable, change in porosity does not affect the pressure drop as significantly high as occurs in the no slip case. Basically, in the case of 50 nm slip length, a slight difference on the pressure drop with respect to the porosity change exists. This result is visually supported in Figure 5 (c,f,i, and l) by overlooking at the pressure contours for different porosity values with 50 nm slip length. As porosity increases, sharp changes in pressure exist, specifically at the corners of the representative volume, and this is more evident for the case with 50 nm slip length. Although the existence of high pressure drops at the corners becomes insignificant for the smaller porosity values for no slip case, with the presence of slip velocity, the sharp pressure drop is still observed in slip flow for low porosity values. As seen in, the case with 50 nm slip length, pressure drops more drastically at the corner for porosity of 0.32 than flow with a 5-nm slip length. However, for the same porosity of REV, pressure drop through the void space is almost linear for the no slip flow. The streamlines show that flow field experiences different models with respect to the porosities present at the specified domains. With different porosities, various secondary flows occur in some parts of the geometry. The numbers of secondary flows differ in accordance with the porosity. Moreover, slip condition also influences the number of secondary flows, for lower porosities. For instance, for porosity of 0.32, no slip and 5 nm slip conditions undergo three and two pieces of secondary flow patterns, respectively.

Also, an increase in porosity provides larger empty spaces for flow through top and bottom, and consequently the quantity of secondary flows diminishes. Due to the high amount of fluid flow entering the top and bottom regions vortices tend to divide the flow into two secondary flows.

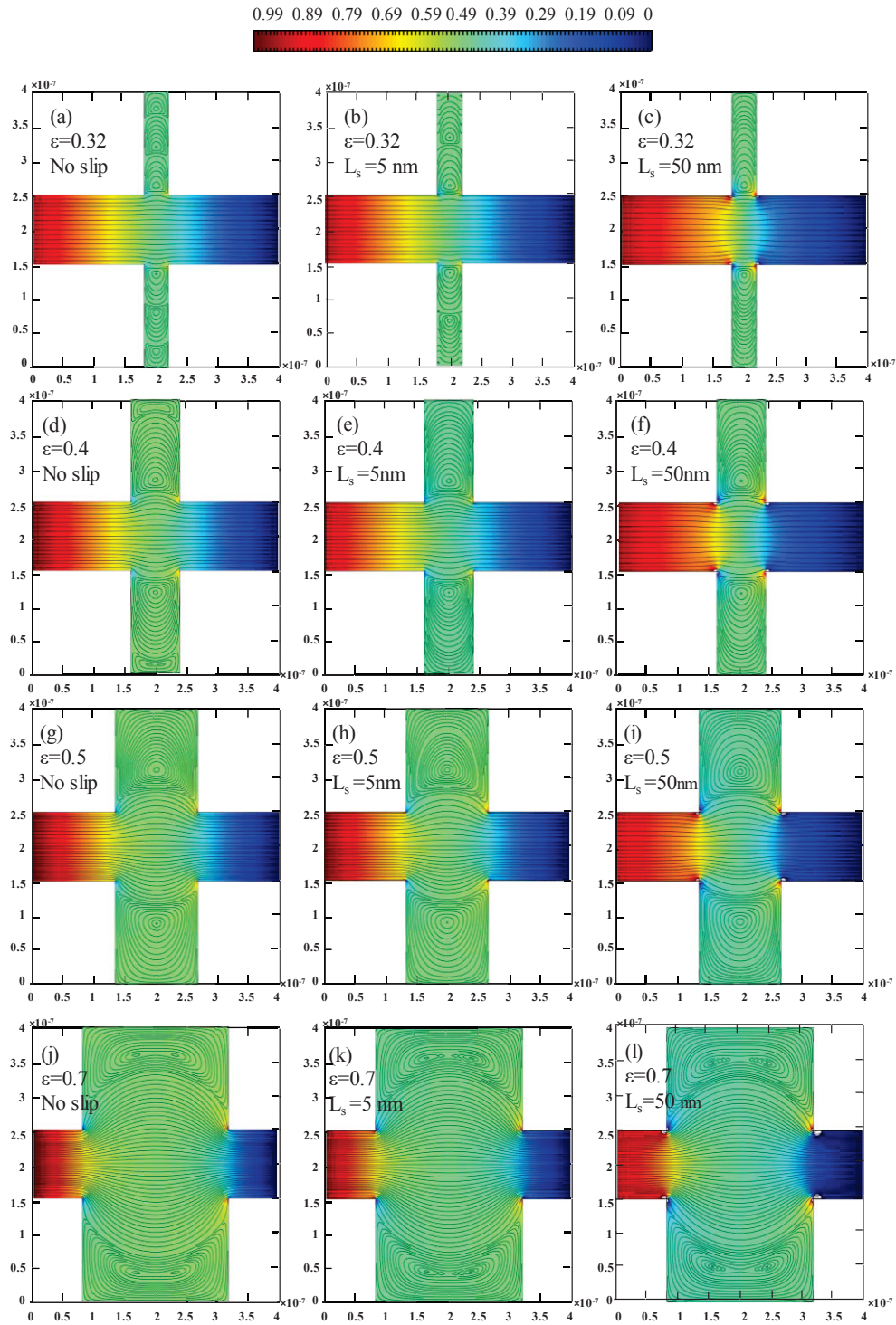


Figure 5.7. Representation of streamlines and pressure contours in the considered domain for a specified  $R_{pt}=4$  with slip and no slip boundary conditions.

The variation in the dimensionless pressure drop and dimensionless permeability values with respect to different values of porosities are represented in Figure 5.8 by taking slip effect into consideration. Due to the structural limitations, porosity range could not have been kept constant, thus, not all the values of porosity are applicable for any given  $R_{pt}$  values. A broad range of porosity investigation could only be possible for the highest  $R_{pt}$  value, which is equal to 10 in this study. The lower and upper porosity values that were investigated for the corresponding  $R_{pt}$  values are listed in Table 5.1.

Table 5.1. Lower and upper limits of porosity values for determined pore to throat size ratios.

Pore to throat size ratio	Porosity range
10	0.1-0.91
6.66	0.15-0.91
4	0.25-0.92
3.39	0.3-0.93
2.6	0.39-0.94
2	0.5-0.95

The smallest porosity values of each different  $R_{pt}$  values are determined by considering the flow geometry as a channel. The variation in the flow domain with varying porosities for a constant  $R_{pt}$  equal to 2 can be visualized in Figure 5.8 (a). Figure 5.8 (a&b) exhibit the result of solution with no slip boundary conditions, while Figure 5.8 (c&d) and (e&f) are drawn with the results of slip flow solution with slip length values of 5 nm and 50 nm, respectively. In this study, all results are evaluated with Re number less than 1 to be able to use Darcy's Law, and as it well known, the solution of Darcy's Law indicates that there is a linear relation between non-dimensional pressure drop and inverse of non-dimensional permeability values (Eq. 3.25). In order to observe this relation, dimensionless pressure drop and dimensionless permeability values are merged into the figure together. Results showed that, as the porosity increases, namely, increase in void volume where fluid flow occurs, non-dimensional pressure drop of porous medium decreases, hence permeability increases. Also, it is consistent for both no slip and slip conditions that permeability values of porous media decrease as the value of  $R_{pt}$  increases since the throat sizes become smaller, the impact of throat on the flow gains

significance on the pressure gradient. Although the general response of permeability to the change in  $R_{pt}$  values is the same, the slopes of the measured permeability values differ due to the impact of slip velocity. In the no slip case, for a specific  $R_{pt}$ , non-dimensional permeability values increase in a very sharp trend as the porosity increases. However, the change in permeability becomes flatter for the slip flow condition. It is clear that for a constant  $R_{pt}$  value, a change in the permeability is almost flat when porosity changes. In the case where slip flow is dominant, the change in accordance with the  $R_{pt}$  is more dominant on the flow than the change in porosity. Additionally, slip effect results in a considerable increase on the permeability of the representative volume.

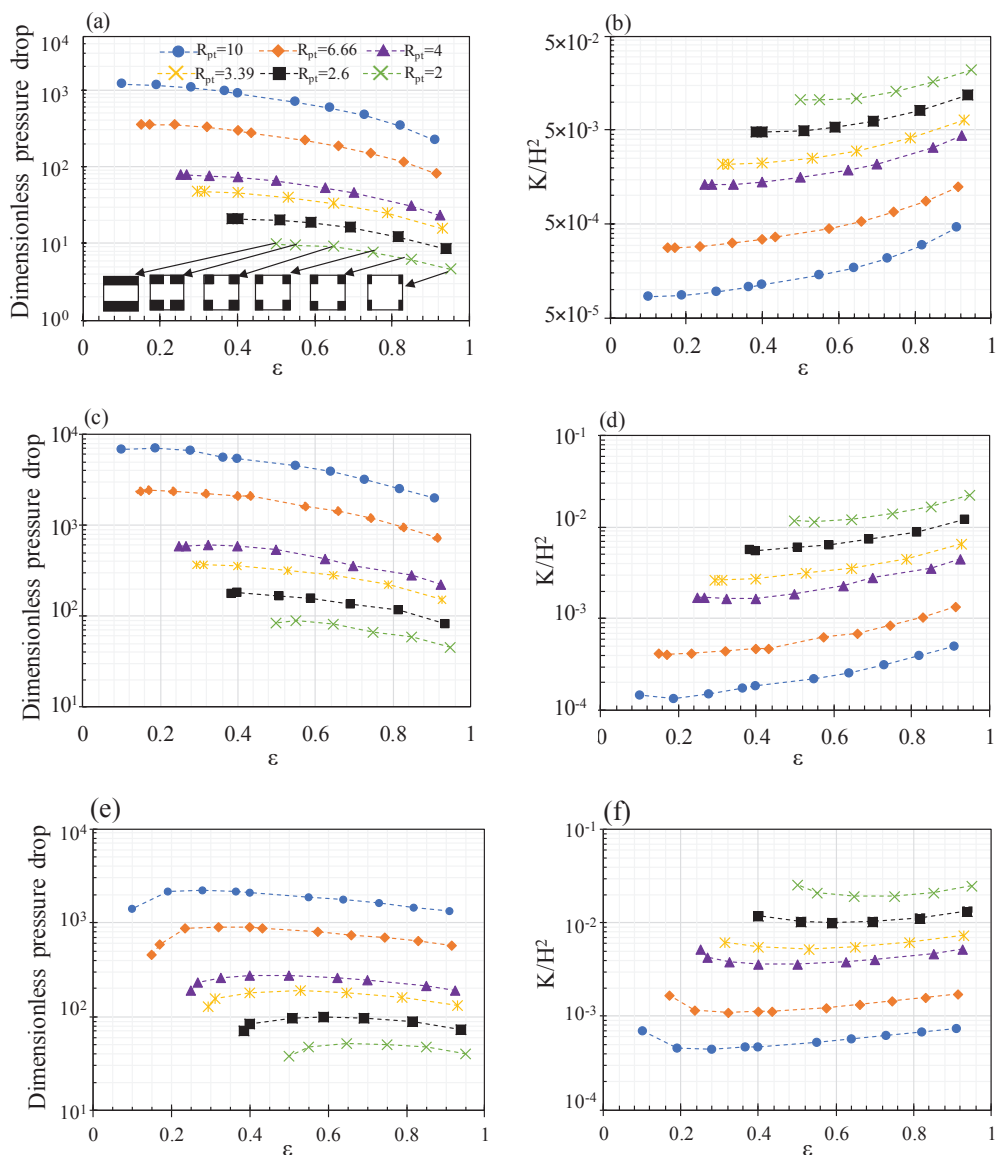


Figure 5.8. The variation in dimensionless pressure gradient and dimensionless permeability values with different porosities. (Figures (a&b), (c&d), and (e&f) represent no slip, slip with 5 nm and 50 nm slip length results, respectively.)

For a better observation of slip effect on the permeability of considered porous media, permeability values are evaluated in the geometry with  $R_{pt}$  values are equal to 4 and 10, and represented in Figure 5.9. (a) and (b), respectively. As the pore to throat size increases from the value of 4 to 10, permeability of porous medium decreases approximately by 10-fold. However, in the presence of high slip effect at the boundaries, for instance flow with 50 nm slip length at the pore surface-fluid boundary, the amount of decrement is also reduced. As indicated in the previous paragraph, the effect of slip results in the change in slope of the relation between permeability and porosity. Based on Kozeny-Carman's proposal, a linear relation between porosity and permeability values is expected. However, it is found that as the effect of slip included to the flow, the relationship between permeability and porosity diverges from linearity, and changes for different  $R_{pt}$  values and slip lengths. The extreme case with 50 nm slip length at different  $R_{pt}$  values represents a clear divergence from linear behavior. Hence, based on those differences in permeability-porosity relation in the presence of different  $R_{pt}$  and slip length values, it is decided to re-visit Kozeny-Carman equation by including slip effects into the calculation of Kozeny Carman Constant.

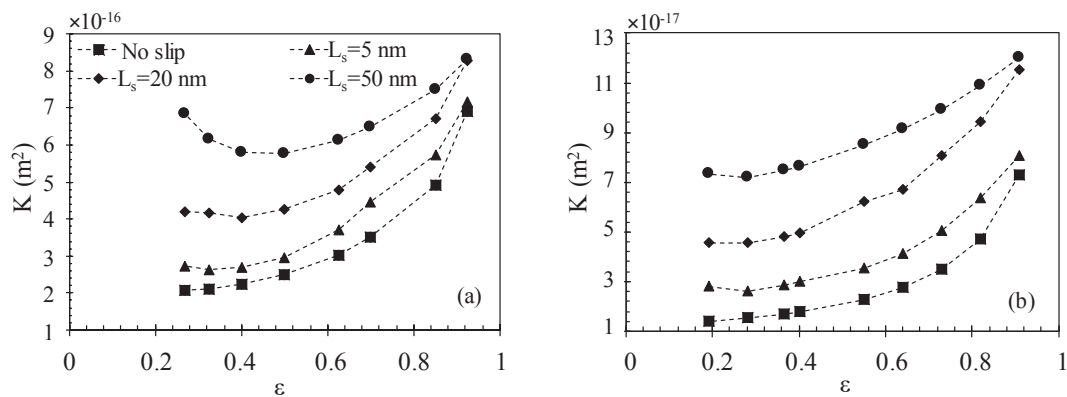


Figure 5.9. Permeability-porosity relation with different slip conditions and pore to throat size ratio. (a)  $R_{pt}=4$ , and (b)  $R_{pt}=10$

## 5.2. Calculations of Kozeny Carman Constant

Up to this section of the study, all evaluations were completed based on Darcy's Law, hence specifically,  $H$  value of the specified domain was used in order to obtain dimensionless permeability values. On the other hand, for the investigation of Kozeny Carman constant, permeability should be identified based on hydraulic diameter (Eq.

3.12) as shown in Kozeny-Carman equation (Eq. (3.13)). Ozgumus and co-workers proposed a relation between Kozeny Carman constant and porosity which exhibited the variation on Kozeny Carman constant as a function of power of porosity;

$$C_{KC} = C_1 \varepsilon^{C_2} \quad (5.2)$$

Where coefficients of  $C_1$  and  $C_2$  are identified as functions of  $R_{pt}$ . This study was performed with the no slip boundary conditions. A similar attempt was made to determine whether this relation is still valid for the slip flow. For this purpose, Kozeny Carman constant ( $C_{KC}$ ) was re-examined by considering it as a function of both porosity and  $R_{pt}$ , and relation between  $C_{KC}$  at different  $R_{pt}$  values and porosities is investigated for the slip flow with 5 nm and 50 nm slip length, and also in the no slip case. As observed in Figure 5.10, the relation between  $C_{KC}$  and porosity is still valid for the slip flow similar to the behavior which was observed in no-slip flow. This figure mainly shows that  $C_{KC}$  take different values with differing  $R_{pt}$  values, and hence  $C_{KC}$  should be defined as a function of both  $\varepsilon$  and  $R_{pt}$ .

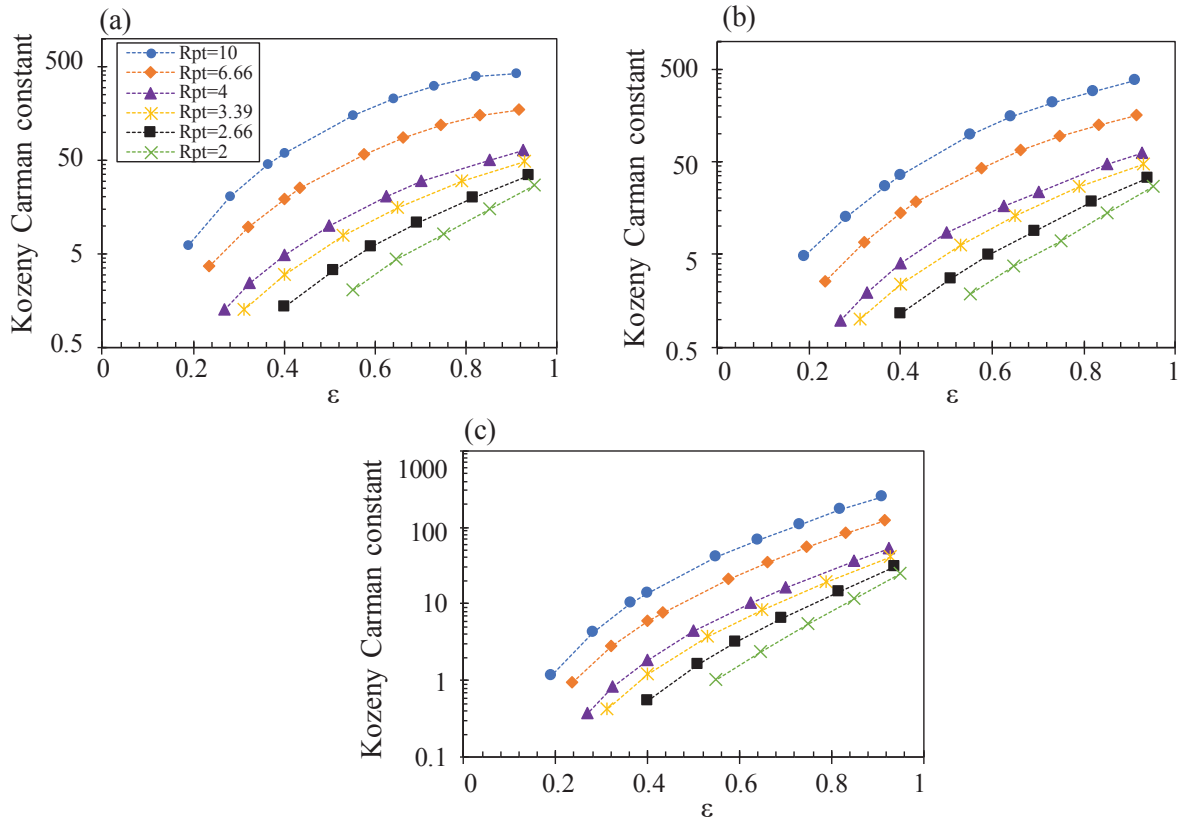


Figure 5.10. Change in  $C_{KC}$  with porosity for different  $R_{pt}$  values at (a) no slip, (b)  $L_s=5\text{nm}$ , (c)  $L_s=50\text{ nm}$ .

By considering the relation between  $C_{KC}$  and porosity, the coefficients of the proposed model, namely  $C_1$  and  $C_2$  can be identified as a function of  $R_{pt}$  as follows;

$$C_1 = c_{11}R_{pt}^2 + c_{12}R_{pt} + c_{13} \quad (5.3)$$

$$C_2 = c_{21}R_{pt}^{c_{22}} + c_{23} \quad (5.4)$$

Where coefficients  $c_{11}$ ,  $c_{12}$ ,  $c_{13}$ ,  $c_{21}$ ,  $c_{22}$ , and  $c_{23}$  varies with respect to the value of  $L_s$  as they can be given in Table 5.2.

Table 5.2. The empirical coefficients for the evaluation of Kozeny Carman Constant

$L_s$ (nm)	$c_{11}$	$c_{12}$	$c_{13}$	$c_{21}$	$c_{22}$	$c_{23}$
0	10.96	-44.46	82.96	12.71	-2.73	2.86
5	5.58	-6.87	21.20	8.20	-1.97	2.80
50	3.01	2.57	11.26	8.47	-1.93	3.40

Kozeny Carman Constant values are re-evaluated by using proposed model (Eq. 5.2) and the comparison between porosity values obtained from proposed model, and the values used in the calculations are done. Figure 5.11 (a), (b), and (c) are drawn for no slip, and slip length with 5 nm and 50 nm, respectively, in order to observe the behavior in the existence of different slip conditions. An almost linear relation between the terms of  $16Kk_c/d_h^2$  and  $\epsilon$  is observed for both no slip, and slip flow cases. Also, as shown, results based on comparison become more linear as the slip length increases.

As it can be seen, KC equation can be applicable in case of liquid slip. In the next chapter, the behavior of permeability with respect to change of slip at different porosity and  $R_{pt}$  values will be investigated. By this way, an extension of the KC model for liquid slip will be attempted.



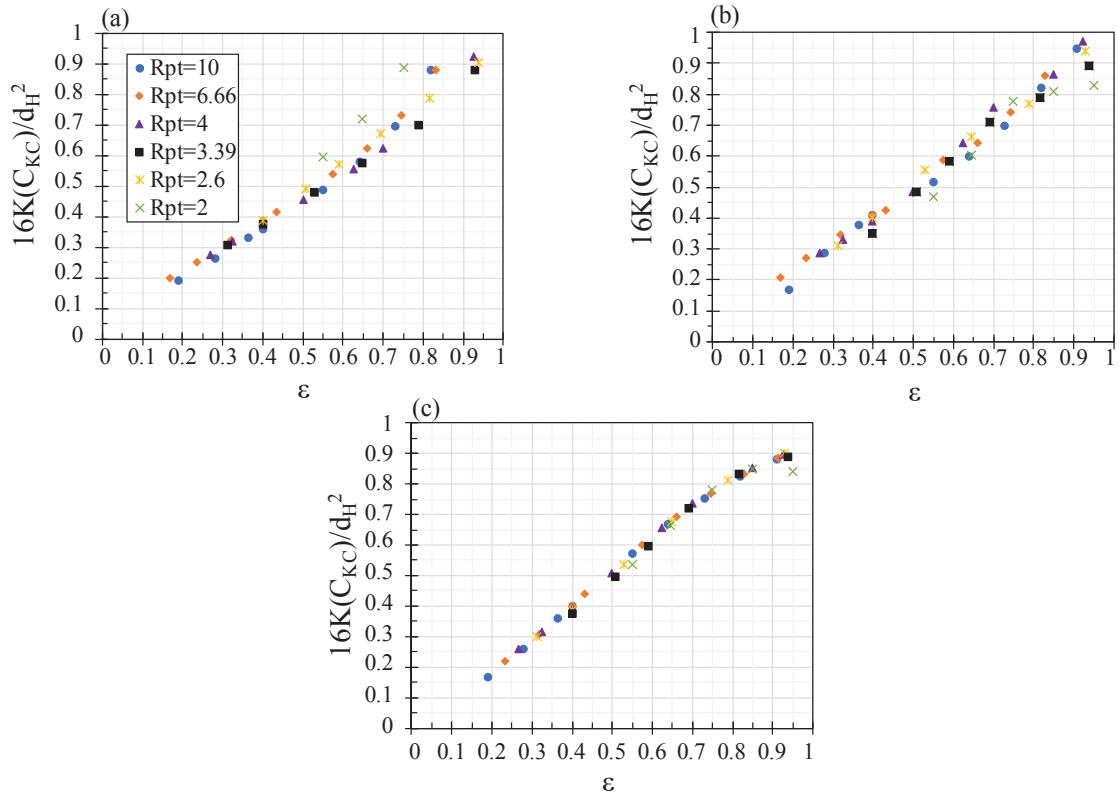


Figure 5.11. Comparison between the results of proposed model and Kozeny-Carman equation (a)no slip, (b)  $L_s=5$  nm, and (c)  $L_s=50$  nm.

### 5.3. Extend of Kozeny Carman Model for Liquid Slip

In the previous section, KC equation was applied both for no slip and slip flow cases. As expected, the deviations were observed between no slip and slip flow case in the Kozeny Carman Constant model. Therefore, it is evident that the slip flow effect should be included in addition to effect of  $R_{pt}$  into the  $C_{KC}$  model. However, it was determined that it would be rather difficult to re-model the parameters in order to construct a new model for  $C_{KC}$  that includes both the influence of slip effects and  $R_{pt}$ . Instead, our aim was to develop an extension as an addition to the KC model. For this purpose, in order to observe the direct relation between slip length and permeability, the dimensional form of mentioned parameters is plotted and it can be seen in Figure 5.12, with respect to varying porosity values in the range of 0.3 and 0.8, for different values of  $R_{pt}$ . It can be clearly extracted from the figure that, increasing the slip length causes significant increase in the permeability values. Particularly, for the small values of  $R_{pt}$  and porosity, when  $R_{pt}=2.6$  and  $\epsilon=0.4$ , slip effect is more dominant and it causes more

dramatic increase in the permeability values, in comparison to the relatively higher values of  $R_{pt}$  and porosity. Moreover, the linear relation between slip length and permeability which was particularly observed for the small values of  $R_{pt}$  and porosity turns into the 2<sup>nd</sup> order parabolic function as the  $R_{pt}$  values increase. It can be claimed that it was an expected behavior, since for the small values of  $R_{pt}$  and porosity, the flow domain resembles a channel geometry, where slip effects are majorly observed due to the presence of high surface area affected by the slip length in such cases.

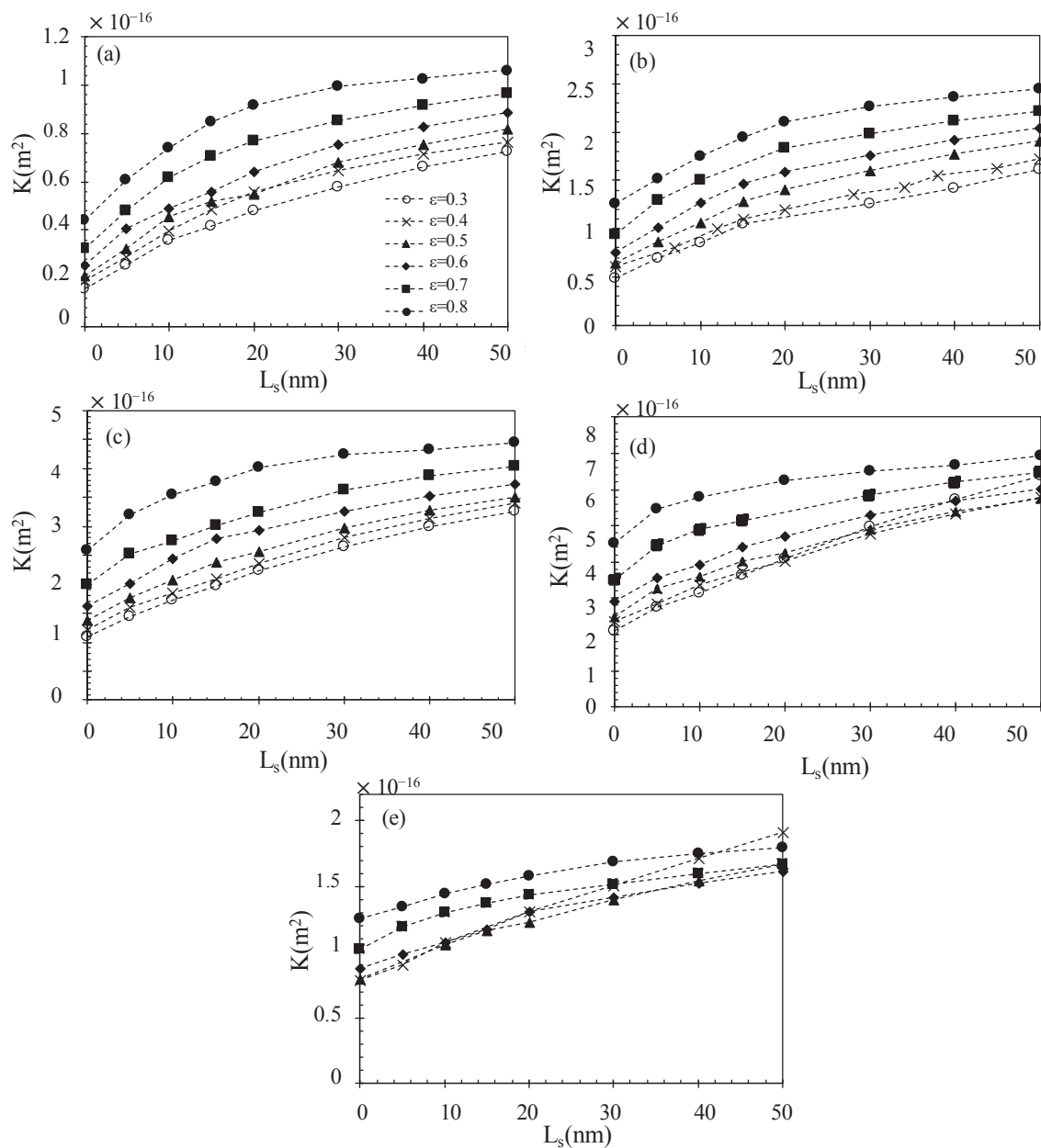


Figure 5.12. Permeability variation with respect to slip length ( $L_s$ ) for (a)  $R_{pt} = 10$  (b)  $R_{pt} = 6.66$  (c)  $R_{pt} = 5$ , (d)  $R_{pt} = 4$ , and (e)  $R_{pt} = 2.6$

In order to observe the trend in the permeability variation in accordance with the slip length, results belonging to the non-dimensional forms of permeability and slip length values are represented in Figure 5.13. Permeability values are normalized with the no slip permeability values obtained from the KC relation, and slip length values are normalized by dividing the  $L_s$  to the height of the REV ( $H$ ). Although several alternatives for the normalization of slip length values exist, such as pore size or throat size; using the dimension of REV is found as more feasible in comparison to the other alternatives. The decrease in permeability with the increase of porosity can be observed clearly in this figure. As the porosity increases, the increment trend with respect to the slip coefficient diverges from linearity and turn into the parabolic behavior, since the effect of slip reduces due to the decrease in solid surfaces which influenced by the slip effects for the high porosities. Although it is possible to construct a relation between non-dimensional permeability and slip coefficient, this would not be a universally applicable relation, since the equation cannot give the decent result for  $\beta=0$ . Therefore, further consideration is needed to obtain universal relation which is applicable for each  $\beta$  values.

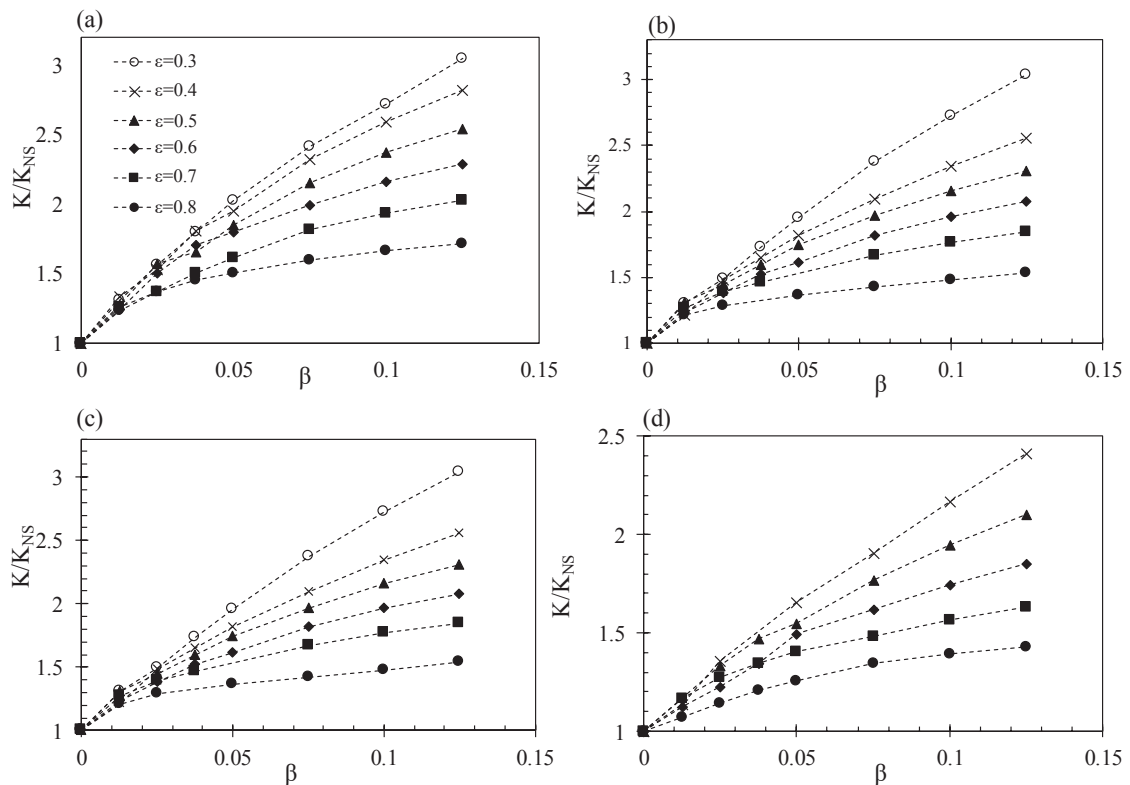


Figure 5.13. Variation in the non-dimensional permeability values and slip coefficient for (a)  $R_{pt}=10$ , (b)  $R_{pt}=5$ , (c)  $R_{pt}=4$ , (d)  $R_{pt}=2.6$ .

In order to model permeability as an extension of KC relation with the slip correction, the similar approach has been done in the gaseous flow in the porous media is re-visited. Klinkenberg is firstly introduced the slip correction for the gaseous flow as follows; (Klinkenberg,1941)

$$k_a = k_\infty f_c \quad (5.5)$$

where,  $k_a$  and  $k_\infty$  represent the gas and liquid permeabilities respectively, and  $f_c$  is the correction factor. Klinkenberg is defined this slip correction as a function of Knudsen number (Kn) as it can be found as Eq. 5.6.

$$f_c = 1 + \frac{b_k}{p} = 1 + 4Kn \quad (5.6)$$

where  $b_k$  is the Klinkenberg's slippage factor and  $p$  is the pressure. After Klinkenberg's model, the correction factor  $f_c$  is tried to be re-modeled in different manners. More recently, Civan (Civan,2010) proposed that this correction factor can be defined as an inverse power function of Kn number (Eq. 5.8) by using the 2<sup>nd</sup> order slip model which has been discussed by Beskok and Karniadakis (Beskok and Karniadakis, 1999). For gaseous flow, as a general approach, 1<sup>st</sup> order slip is used, whereas for the cases where different non-equilibrium behaviors are observed, 2<sup>nd</sup> order slip model is proposed with the viscosity correction in order to predict the case that velocity profiles are still in parabolic shape. When it comes to the liquid flow, the 2<sup>nd</sup> order slip model can also be used, although the need for the update of the viscosity is not required, since the viscosity remains constant for the liquid flow. The 2<sup>nd</sup> order slip model developed by Beskok and Karniadakis can be written for a fully diffused case where accommodation coefficient is equal to 1, and coefficient  $b$  in the original form of the equation is indicated as -1 with the Direct Simulation Monte Carlo results as follows;

$$U_s - U_w = \frac{Kn}{1 + Kn} \left( \frac{\partial U}{\partial n} \right)_s \quad (5.7)$$

$$b_k = 0.0094 \left( \frac{K_\infty}{\varepsilon} \right)^{-1/2} \quad (5.8)$$

In the light of those approaches, a phenomenological model in the current study is built as follows;

$$\frac{K - K_{NS}}{K_{NS}} = A \times \left( \frac{\beta}{1 + \beta} \right)^B \quad (5.9)$$

Where A and B are coefficients which are going to be defined as a function of both porosity and permeability as it will be discussed further. The only limitation about this proposed model is the dimensional limitations due to the near surface non-equilibrium (i.e. Electrical Double Layer and density layering). The non-dimensional permeability variation with respect to non-dimensional slip length, referred to as coefficient ( $\beta$ ) can be found in the Figure 5.13 for different specified  $R_{pt}$  values and varying porosities. It is worth to stating that, although the polynomial fitting options also exhibit decent fitting for the curves, the asymptotic value which are the permeability results when  $\beta \rightarrow \infty$  could not be reached for this kind of fitting. This means that, using such polynomial model causes erroneous predictions for the permeability in the slip flow. As illustrated in Figure 5.14, all values are almost perfectly matched with the power function fitting, and the trend provides reasonable results in the possible range of  $\beta$ . For each specified  $R_{pt}$  value, the relation between permeability and slip length is investigated by changing porosities. By that, the model can be examined as both functions of porosity and  $R_{pt}$ . In the fitting functions given in the plots, y and x represent  $\frac{(K - K_{NS})}{K_{NS}}$  and  $\frac{(\beta + 1)}{\beta}$ , while the multiplier coefficient and power coefficients are the terms which are denoted as A and B in the Eq 5.9, respectively.

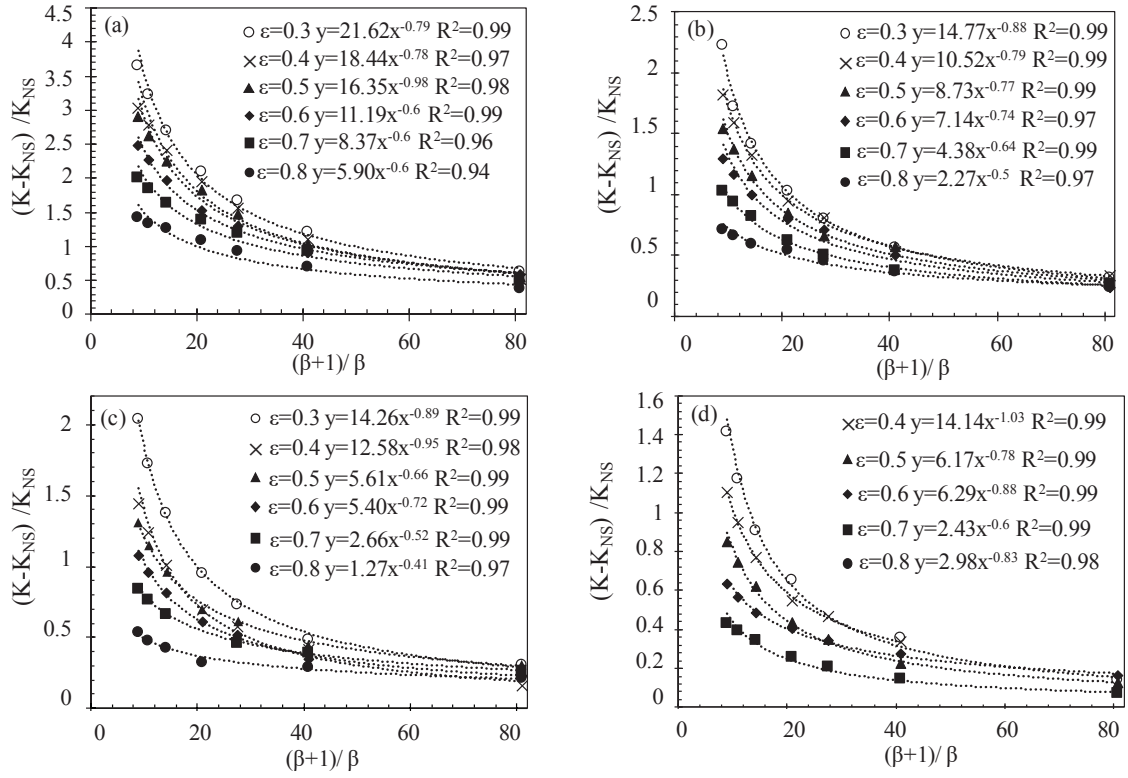


Figure 5.14. The relation between non-dimensional permeability and slip coefficient and the fitting trend lines with different  $R_{pt}$  values as (a)  $R_{pt}=10$  (b)  $R_{pt}=5$  (c)  $R_{pt}=4$ , and (d)  $R_{pt}=2.6$ . Dashed lines represent the fitting trend line.

It is clearly seen in Figure 5.14, a linear relation between the coefficients of the main relation given in the Eq. 5.9 and porosity exist. Based on this observation, those mentioned A and B coefficients in the fitting functions, are collected, and they are re-drawn with respect to porosity in Figure 5.15, to determine the coefficients as a function of porosity. Basically, A and B coefficients can be related with porosity as,

$$A = a_{11}\varepsilon + a_{12} \quad (5.10)$$

$$B = b_{11}\varepsilon + b_{12} \quad (5.11)$$

The predicted linear relationship can be supported with the high values of regression coefficients which are given in Figure 5.15. The values of the coefficients  $a_{11}$ ,  $a_{12}$ ,  $b_{11}$ , and  $b_{12}$  can be found for each case in the Figure 5.15.

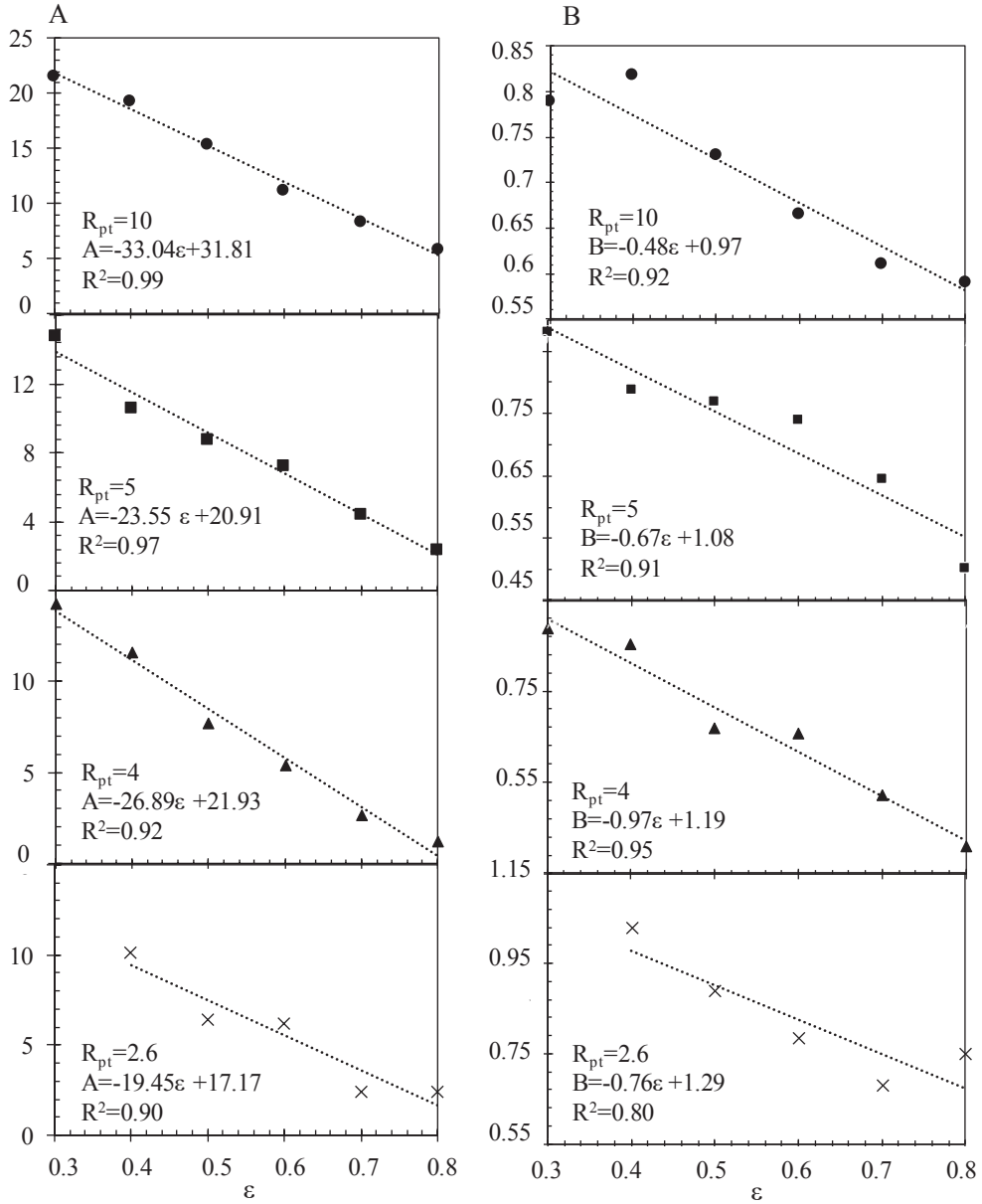


Figure 5.15. Fitting functions of coefficients A (left) and B (right) as a function of porosity for a specific  $R_{pt}$ .

The last step for obtaining the proposed phenomenological model for the extension of KC relation with the slip correction as a function of both porosity,  $R_{pt}$  is to derive a relation between  $R_{pt}$  and the coefficients in Eqs. (5.10) and (5.11). Similar linear relation can be written as below based on the linear relation seen in Figure 5.16.

$$a_{11} = a_{111}R_{pt} + a_{112} \quad (5.12)$$

$$b_{11} = b_{111}R_{pt} + b_{112} \quad (5.13)$$

$$a_{12} = a_{121}R_{pt} + a_{122} \quad (5.14)$$

$$b_{12} = b_{121}R_{pt} + b_{122} \quad (5.15)$$

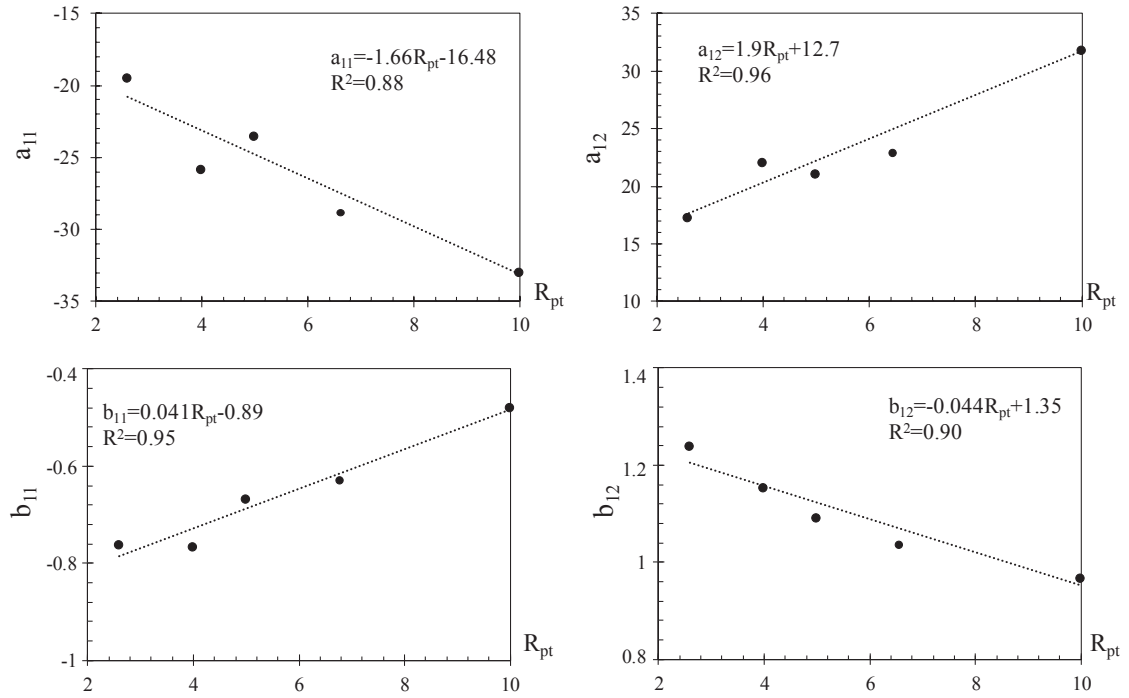


Figure 5.16. Coefficients in Eq. (5.10) and (5.11) as a function of  $R_{pt}$ .

After all those derivations, the final form of the derived model can be written as follows,

$$K = K_{NS} + K_{NS} \times \left( (-1.66 \times R_{pt} \times \varepsilon - 16.48 \times \varepsilon + 1.9 \times R_{pt} + 12.7) \times \left( \frac{\beta}{1 + \beta} \right)^{(0.041 \times R_{pt} \times \varepsilon - 0.89 \times \varepsilon - 0.044 \times R_{pt} + 1.35)} \right) \quad (5.16)$$

With the help of Eq. (5.16) for square rod geometries, permeability values can be predicted by calculating no slip permeability values via Kozeny Carman equation. In order to check the validity of the model, the permeability values obtained straightforward by using Darcy's Law with the simulation results of velocity and pressure values, and result obtained with the proposed model are compared and drawn against different  $R_{pt}$  values in Figure 5.17. For the validation, some specific porosity values such as 0.3, 0.5, and 0.7 are selected which may provide better visual observation. Due to the geometrical limitations that were stated before, porosity value of 0.3 could not be drawn for the  $R_{pt}=2.6$  case, since it is physically impossible to construct such a geometry. The good



agreement between the results prove that, permeability values can be computed by using extended form of KC relation with the slip correction.

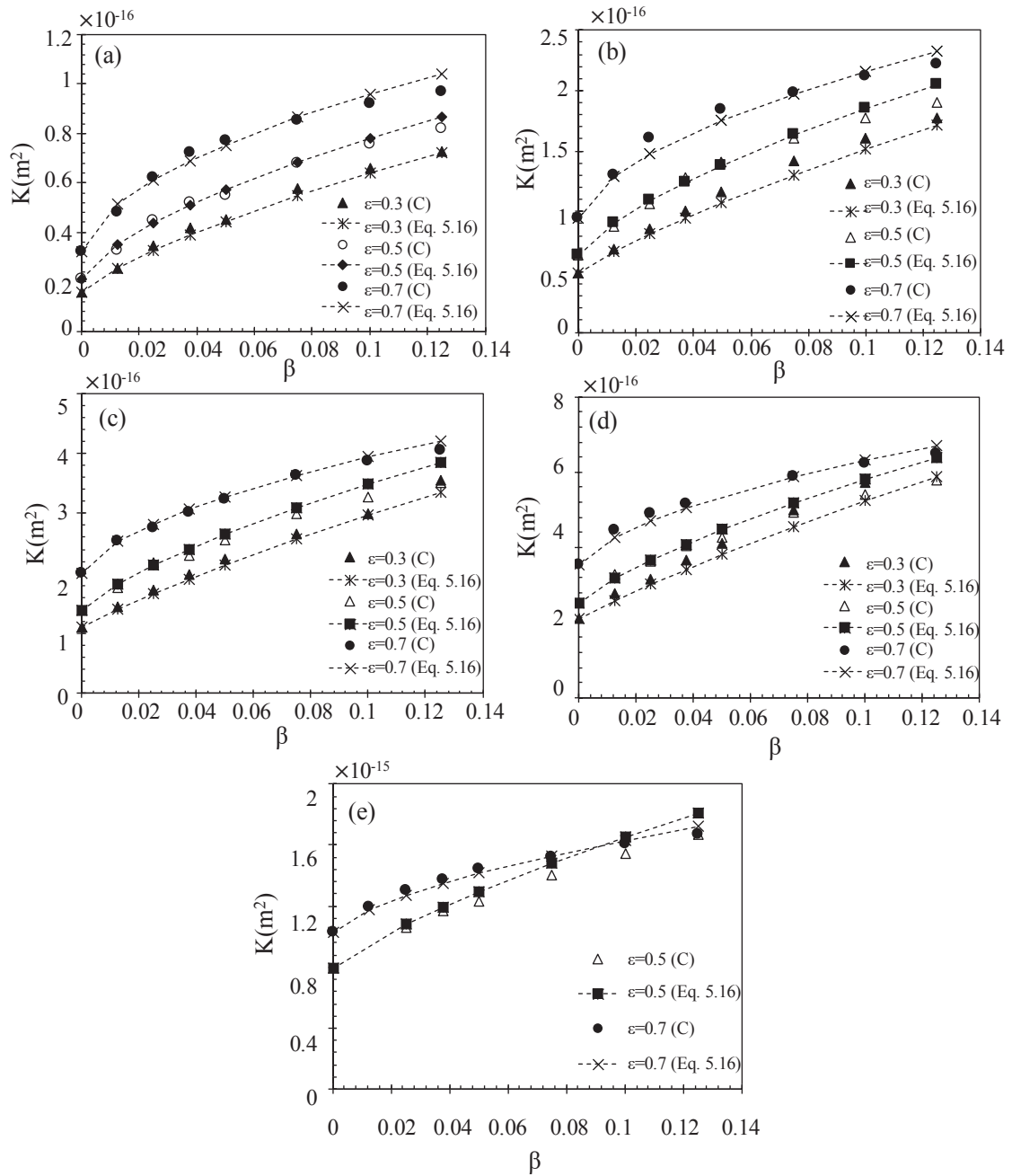


Figure 5.17. Comparison between the simulation results and results of proposed model for permeability as a function of slip coefficient with (a)  $R_{pt}=10$ , (b)  $R_{pt}=5$ , (c)  $R_{pt}=4$ , (d)  $R_{pt}=2.6$ . Notation of (C) and (Eq. 5.16) denote the results of numerical computations, and calculations results of the proposed model, respectively

## CHAPTER 6

### CONCLUSION

There are a vast number of applications of transport in micro/nanoscale porous media. This reveals the need for an investigation of fluid flow characteristics in those systems. To accomplish this, the current study, liquid flow transport in small scale porous media is characterized by considering geometry and non-equilibrium effects on the specified porous media. The effect of non-equilibrium behavior developed due to the small scale was evaluated in terms of slip length. Permeability values of the micro/nanoscale porous media were measured, using pore-level analyses of a representative volume at different porosities, pore-to-throat size ratios ( $R_{pt}$ ) and slip velocity boundary conditions. Additionally, due to the considerable impact of  $R_{pt}$  on the permeability values, Kozeny Carman Constant ( $C_{KC}$ ) was re-defined as a function of both porosity and pore to throat size ratio. It is observed that Kozeny Carman equation that includes the KC constant as a function of both porosity and  $R_{pt}$  is still applicable for slip flow. Hence, an extended Kozeny Carman model to predict permeability values as a function of porosity, pore-to-throat size ratio, and slip coefficient was successfully devised by using numerical computations.

It is important to understand the effect of slip length on permeability in micro/nanoscale porous media, since the previous studies about the area of interest consist of mostly rarefied gas dynamics. For this purpose, a need for liquid transport was recognized and the non-equilibrium behavior was investigated in such systems. A wide literature survey provided the published slip length results of various liquid/solid couples was discussed. Published data with corresponding conduits sizes in an attempt to justify slip coefficient ranges to study were normalized. On the other hand, the required slip values could only be calculated empirically or by molecular simulations, due to the lack of a simple theory. For this case, possible relations between velocity slip and surface wetting in order to estimate the required boundary conditions from an easy contact angle measurement are discussed. Available slip length measurements, accompanied with the wetting angle of corresponding surfaces, and proposed slip versus wetting models were summarized. Based on the available data, slip length showed an exponential increase from

almost negligible values to 10nm in the 50° to 150° contact angle range. It should be underlined here that existing data is very limited and slip length values much higher than those were also stated in the literature without the corresponding contact angle values. In the light of these, two different slip length values as 5 nm and 50 nm were selected in order to observe the effect of slip on the system. It was seen that as the slip effect increased due to the significant decrease in the friction, pressure drop decreases, and consequently permeability values increase.

Different than most of the existing studies, the significant role of the throat size on the permeability values was considered in this study, and it is seen that defining permeability only by porosity results in wrong transport predictions. Parametric study results show that, for a given porosity, permeability values show variation by connectivity, average-size and wetting condition of the porous system. The increase in the permeability was observed as  $R_{pt}$  decreases since the flow domain resembles channel flow. On the contrary, permeability values decreased as the value of  $R_{pt}$  is changed from 2 to 10 since the main flow is influenced by the secondary flows which resulted in a decrease in the pressure drop.

Based on the clear observation of how permeability was affected by slip, a model was developed where permeability in the presence of slip is contributed by the no slip permeability that was calculated via KC equation, a non-dimensional slip length term, and the coefficients as the functions of both porosity and  $R_{pt}$ . In order to estimate the behavior of the model, curve fitting was performed and inverse power law was implemented, since it was found to satisfy the asymptotic results. The coefficients of the proposed model were re-defined with respect to porosity and  $R_{pt}$  successively. The computational results and the results obtained via model were in a good agreement. For the final step, for a specified square rod geometry, the final model was devised to provide the permeability values for given porosity and  $R_{pt}$  and slip length.

For a future study, the model can be investigated for different types of pore geometries and arrangements. Specifically, shape effects including tortuosity can be defined as a function of porosity and the proposed model can be re-visited with the consideration of the tortuosity for a better understanding of the effects of geometrical aspects on the flow characteristics.

## REFERENCES

- Adler, P. M. "Fractal porous media III: Transversal Stokes flow through random and Sierpinski carpets." *Transport in Porous Media* 3, no. 2 (1988): 185-198.
- Afsharpoor, Ali, and Farzam Javadpour. "Liquid slip flow in a network of shale noncircular nanopores." *Fuel* 180 (2016): 580-590.
- Akbarinia, A., Morteza Abdolzadeh, and R. Laur. "Critical investigation of heat transfer enhancement using nanofluids in microchannels with slip and non-slip flow regimes." *Applied Thermal Engineering* 31, no. 4 (2011): 556-565.
- Appiah, Francis, Farzam Javadpour, and Rouzbeh Ghanbarnezhad Moghanloo. "Apparent liquid permeability in shale." In *Unconventional Resources Technology Conference*, pp. 2496-2512. Society of Exploration Geophysicists, American Association of Petroleum Geologists, Society of Petroleum Engineers, 2013.
- Baban, Dilair F., and Leonard W. Seymour. "Control of tumour vascular permeability." *Advanced drug delivery reviews* 34, no. 1 (1998): 109-119.
- Bahga A., Madiseti, V. K., Desai, B.G., Sircar A., "In-situ permeability prediction approach for tight gas sandstone reservoir", *Journal of Energy and Management* 1, no. 1(2016): 3-24
- Bardia, Raunak, Zhi Liang, Pawel Keblinski, and Mario F. Trujillo. "Continuum and molecular-dynamics simulation of nanodroplet collisions." *Physical Review E* 93, no. 5 (2016): 053104.
- Barisik, Murat, and Ali Beskok. "Boundary treatment effects on molecular dynamics simulations of interface thermal resistance." *Journal of Computational Physics* 231, no. 23 (2012): 7881-7892.
- Barrat, Jean-Louis, and Lydéric Bocquet. "Large slip effect at a nonwetting fluid-solid interface." *Physical review letters* 82, no. 23 (1999): 4671.
- Beskok, Ali, and George Em Karniadakis. "Report: a model for flows in channels, pipes, and ducts at micro and nano scales." *Microscale Thermophysical Engineering* 3, no. 1 (1999): 43-77.
- Bo-Ming, Yu, and Li Jian-Hua. "A geometry model for tortuosity of flow path in porous media." *Chinese Physics Letters* 21, no. 8 (2004): 1569.
- Boving, Thomas B., and Peter Grathwohl. "Tracer diffusion coefficients in sedimentary rocks: correlation to porosity and hydraulic conductivity." *Journal of Contaminant Hydrology* 53, no. 1 (2001): 85-100.
- Brown, S. G. R., J. A. Spittle, D. J. Jarvis, and R. Walden-Bevan. "Numerical determination of liquid flow permeabilities for equiaxed dendritic structures." *Acta materialia* 50, no. 6 (2002): 1559-1569.

- Buongiorno, Jacopo. "Convective transport in nanofluids." *Journal of Heat Transfer* 128, no. 3 (2006): 240-250.
- Byun, Doyoung, Jihoon Kim, Han Seo Ko, and Hoon Cheol Park. "Direct measurement of slip flows in superhydrophobic microchannels with transverse grooves." *Physics of Fluids* 20, no. 11 (2008): 113601.
- Cao, Bing-Yang, Min Chen, and Zeng-Yuan Guo. "Liquid flow in surface-nanostructured channels studied by molecular dynamics simulation." *Physical Review E* 74, no. 6 (2006): 066311.
- Cao, Zhe, Guangdi Liu, Hongbin Zhan, Chaozheng Li, Yuan You, Chengyu Yang, and Hang Jiang. "Pore structure characterization of Chang-7 tight sandstone using MICP combined with N2GA techniques and its geological control factors." *Scientific reports* 6 (2016): 36919.
- Carman, Phillip C. "Fluid flow through granular beds." *Transactions-Institution of Chemical Engineers* 15 (1937): 150-166.
- Carman, Phillip C. "Permeability of saturated sands, soils and clays." *The Journal of Agricultural Science* 29, no. 02 (1939): 262-273.
- Chen, Xiaoming, and Thanasis D. Papathanasiou. "On the variability of the Kozeny constant for saturated flow across unidirectional disordered fiber arrays." *Composites Part A: Applied Science and Manufacturing* 37, no. 6 (2006): 836-846.
- Chen, Yongping, Chaoqun Shen, Pengfei Lu, and Yongping Huang. "Role of pore structure on liquid flow behaviors in porous media characterized by fractal geometry." *Chemical Engineering and Processing: Process Intensification* 87 (2015): 75-80.
- Cheng, J-T., and N. Giordano. "Fluid flow through nanometer-scale channels." *Physical review E* 65, no. 3 (2002): 031206.
- Cho, Jae-Hie J., Bruce M. Law, and François Rieutord. "Dipole-dependent slip of Newtonian liquids at smooth solid hydrophobic surfaces." *Physical review letters* 92, no. 16 (2004): 166102.
- Choi, Chang-Hwan, and Chang-Jin Kim. "Large slip of aqueous liquid flow over a nanoengineered superhydrophobic surface." *Physical review letters* 96, no. 6 (2006): 066001.
- Choi, Chang-Hwan, K. Johan A. Westin, and Kenneth S. Breuer. "Apparent slip flows in hydrophilic and hydrophobic microchannels." *Physics of fluids* 15, no. 10 (2003): 2897-2902.
- Chun, Myung-Suk, and Sangwoo Lee. "Flow imaging of dilute colloidal suspension in PDMS-based microfluidic chip using fluorescence microscopy." *Colloids and Surfaces A: Physicochemical and Engineering Aspects* 267, no. 1 (2005): 86-94.
- Civan, Faruk. "Effective correlation of apparent gas permeability in tight porous media." *Transport in porous media* 82, no. 2 (2010): 375-384.

- Cohen-Tanugi, David, and Jeffrey C. Grossman. "Water desalination across nanoporous graphene." *Nano letters* 12, no. 7 (2012): 3602-3608.
- Cohen-Tanugi, David, and Jeffrey C. Grossman. "Water permeability of nanoporous graphene at realistic pressures for reverse osmosis desalination." *The Journal of chemical physics* 141, no. 7 (2014): 074704.
- Costa, Antonio. "Permeability-porosity relationship: A reexamination of the Kozeny-Carman equation based on a fractal pore-space geometry assumption." *Geophysical research letters* 33, no. 2 (2006).
- Cottin-Bizonne, C., B. Cross, A. Steinberger, and E. Charlaix. "Boundary slip on smooth hydrophobic surfaces: Intrinsic effects and possible artifacts." *Physical review letters* 94, no. 5 (2005): 056102.
- Cottin-Bizonne, C., S. Jurine, J. Baudry, J. Crassous, F. Restagno, and E. Charlaix. "Nanorheology: an investigation of the boundary condition at hydrophobic and hydrophilic interfaces." *The European Physical Journal E: Soft Matter and Biological Physics* 9, no. 1 (2002): 47-53.
- Craig, Vincent SJ, Chiara Neto, and David RM Williams. "Shear-dependent boundary slip in an aqueous Newtonian liquid." *Physical review letters* 87, no. 5 (2001): 054504.
- Cui, Jiangfeng, Qian Sang, Yajun Li, Congbin Yin, Yanchao Li, and Mingzhe Dong. "Liquid permeability of organic nanopores in shale: Calculation and analysis." *Fuel* 202 (2017): 426-434.
- Darcy, Henry Philibert Gaspard. *Détermination des lois d'écoulement de l'eau à travers le sable*. 1856.
- Dianshi, Xiao., Lu Shuangfang, Lu Zhengyuan, Wenbiao HUANG, and Gu. Meiwei. "Combining nuclear magnetic resonance and rate-controlled porosimetry to probe the pore-throat structure of tight sandstones." *Petroleum Exploration and Development* 43, no. 6 (2016): 1049-1059.
- Discacciati, Marco, and Alfio Quarteroni. "Navier-Stokes/Darcy coupling: modeling, analysis, and numerical approximation." (2009).
- Discacciati, Marco, Edie Miglio, and Alfio Quarteroni. "Mathematical and numerical models for coupling surface and groundwater flows." *Applied Numerical Mathematics* 43, no. 1-2 (2002): 57-74.
- Falk, Kerstin, Felix Sedlmeier, Laurent Joly, Roland R. Netz, and Lydéric Bocquet. "Molecular origin of fast water transport in carbon nanotube membranes: superlubricity versus curvature dependent friction." *Nano letters* 10, no. 10 (2010): 4067-4073.
- Gad-el-Hak, Mohamed. "The fluid mechanics of microdevices-the Freeman scholar lecture." *Transactions-American Society of Mechanical Engineers Journal of Fluids Engineering* 121 (1999): 5-33.

- Gamrat, Gabriel, Michel Favre-Marinet, and Stéphane Le Person. "Numerical study of heat transfer over banks of rods in small Reynolds number cross-flow." *International Journal of Heat and Mass Transfer* 51, no. 3 (2008): 853-864.
- Gao, Hui, Tiantai Li, and Ling Yang. "Quantitative determination of pore and throat parameters in tight oil reservoir using constant rate mercury intrusion technique." *Journal of Petroleum Exploration and Production Technology* 6, no. 2 (2016): 309-318.
- Gao, Zhiye, and Qinhong Hu. "Estimating permeability using median pore-throat radius obtained from mercury intrusion porosimetry." *Journal of Geophysics and Engineering* 10, no. 2 (2013): 025014.
- Ghorbanian, Jafar, and Ali Beskok. "Scale effects in nano-channel liquid flows." *Microfluidics and Nanofluidics* 20, no. 8 (2016): 121.
- Glover, Paul W., and Nicholas Déry. "Streaming potential coupling coefficient of quartz glass bead packs: Dependence on grain diameter, pore size, and pore throat radius." *Geophysics* 75, no. 6 (2010): F225-F241.
- Groombridge, M., M. Schneemilch, and N. Quirke. "Slip boundaries in nanopores." *Molecular Simulation* 37, no. 12 (2011): 1023-1030.
- Heijs, Anton WJ, and Christopher P. Lowe. "Numerical evaluation of the permeability and the Kozeny constant for two types of porous media." *Physical Review E* 51, no. 5 (1995): 4346.
- Heiranian, Mohammad, Amir Barati Farimani, and Narayana R. Aluru. "Water desalination with a single-layer MoS<sub>2</sub> nanopore." *Nature communications* 6 (2015).
- Henderson, Nélio, Juan C. Brêttas, and Wagner F. Sacco. "A three-parameter Kozeny–Carman generalized equation for fractal porous media." *Chemical Engineering Science* 65, no. 15 (2010): 4432-4442.
- Holt, Jason K., Hyung Gyu Park, Yinmin Wang, Michael Stadermann, Alexander B. Artyukhin, Costas P. Grigoropoulos, Aleksandr Noy, and Olgica Bakajin. "Fast mass transport through sub-2-nanometer carbon nanotubes." *Science* 312, no. 5776 (2006): 1034-1037.
- Hooman, K., F. Hooman, and M. Famouri. "Scaling effects for flow in micro-channels: variable property, viscous heating, velocity slip, and temperature jump." *International Communications in Heat and Mass Transfer* 36, no. 2 (2009): 192-196.
- Hooman, Kamel, and Azadeh Ejlali. "Effects of viscous heating, fluid property variation, velocity slip, and temperature jump on convection through parallel plate and circular microchannels." *International Communications in Heat and Mass Transfer* 37, no. 1 (2010): 34-38.
- Huang, David M., Christian Sendner, Dominik Horinek, Roland R. Netz, and Lydéric Bocquet. "Water slippage versus contact angle: A quasiuniversal relationship." *Physical review letters* 101, no. 22 (2008): 226101.

- Huang, Peter, and Kenneth S. Breuer. "Direct measurement of slip length in electrolyte solutions." *Physics of fluids* 19, no. 2 (2007): 028104.
- Jabbarzadeh, A., J. D. Atkinson, and R. I. Tanner. "Wall slip in the molecular dynamics simulation of thin films of hexadecane." *The Journal of chemical physics* 110, no. 5 (1999): 2612-2620.
- Javadpour, F., M. McClure, and M. E. Naraghi. "Slip-corrected liquid permeability and its effect on hydraulic fracturing and fluid loss in shale." *Fuel* 160 (2015): 549-559.
- Jin, Yakang, Xuefeng Liu, Zilong Liu, Shuangfang Lu, and Qingzhong Xue. "Effect of interfacial layer on water flow in nanochannels: Lattice Boltzmann simulations." *Physica B: Condensed Matter* 487 (2016): 18-24.
- Jin-Sui, Wu, and Yin Shang-Xian. "A Micro-Mechanism Model for Porous Media." *Communications in Theoretical Physics* 52, no. 5 (2009): 936.
- Joseph, Pierre, and Patrick Tabeling. "Direct measurement of the apparent slip length." *Physical Review E* 71, no. 3 (2005): 035303.
- Joseph, Pierre, Cecile Cottin-Bizonne, J-M. Benoit, Christophe Ybert, Catherine Journet, Patrick Tabeling, and Lyderic Bocquet. "Slippage of water past superhydrophobic carbon nanotube forests in microchannels." *Physical review letters* 97, no. 15 (2006): 156104.
- Kassinis, S. C., J. H. Walther, E. Kotsalis, and P. Koumoutsakos. "Flow of aqueous solutions in carbon nanotubes." In *Multiscale Modelling and Simulation*, pp. 215-226. Springer Berlin Heidelberg, 2004.
- Khabbazi, A. Ebrahimi, J. Hinebaugh, and A. Bazylak. "Determining the impact of rectangular grain aspect ratio on tortuosity–porosity correlations of two-dimensional stochastically generated porous media." *Science Bulletin* 61, no. 8 (2016): 601-611.
- Khabbazi, A. Ebrahimi, J. S. Ellis, and A. Bazylak. "Developing a new form of the Kozeny–Carman parameter for structured porous media through lattice-Boltzmann modeling." *Computers & Fluids* 75 (2013): 35-41.
- Khaled, A-RA, and K. Vafai. "The role of porous media in modeling flow and heat transfer in biological tissues." *International Journal of Heat and Mass Transfer* 46, no. 26 (2003): 4989-5003.
- Khalili, Arzhang, Bo Liu, Khodayar Javadi, Mohammad R. Morad, Kolja Kindler, Maciej Matyka, Roman Stocker, and Zbigniew Koza. "Application of porous media theories in marine biological modeling." In *Porous Media: Applications in Biological Systems and Biotechnology*, pp. 365-398. (2010): CRC Press.
- Klinkenberg, L. J. "The permeability of porous media to liquids and gases." In *Drilling and production practice*. American Petroleum Institute, 1941.
- Koponen, A., M. Kataja, and J. Timonen. "Permeability and effective porosity of porous media." *Physical Review E* 56, no. 3 (1997): 3319.



- Kou, Zhi Hai, and Min Li Bai. "Effects of wall slip and temperature jump on heat and mass transfer characteristics of an evaporating thin film." *International Communications in Heat and Mass Transfer* 38, no. 7 (2011): 874-878.
- Koumoutsakos, P., R. L. Jaffe, T. Werder, and J. H. Walther. "On the validity of the no-slip condition in nanofluidics." (2003).
- Kozeny, Josef. *Über kapillare leitung des wassers im boden:(aufstieg, versickerung und anwendung auf die bewässerung)*. Hölder-Pichler-Tempsky, 1927.
- Lauga, Eric, Michael P. Brenner, and Howard A. Stone. "Microfluidics: the no-slip boundary condition." (2005): 1-27.
- Lee, Choongyeop, and Chang-Jin "CJ Kim. "Maximizing the giant liquid slip on superhydrophobic microstructures by nanostructuring their sidewalls." *Langmuir* 25, no. 21 (2009): 12812-12818.
- Lee, Kah Peng, Hannah Leese, and Davide Mattia. "Water flow enhancement in hydrophilic nanochannels." *Nanoscale* 4, no. 8 (2012): 2621-2627.
- Li, Long, Jingwen Mo, and Zhigang Li. "Flow and slip transition in nanochannels." *Physical Review E* 90, no. 3 (2014): 033003.
- Lichter, Seth, Ashlie Martini, Randall Q. Snurr, and Qian Wang. "Liquid slip in nanoscale channels as a rate process." *Physical review letters* 98, no. 22 (2007): 226001.
- Lin, M. Y., B. Abeles, J. S. Huang, H. E. Stasiewski, and Q. Zhang. "Viscous flow and diffusion of liquids in microporous glasses." *Physical Review B* 46, no. 17 (1992): 10701.
- Liu, Jinzhou, Qingguo Xue, Xuefeng She, and Jingsong Wang. "Investigation on interface resistance between alternating layers in the upper of blast furnace." *Powder technology* 246 (2013): 73-81.
- Liu, Richeng, Yujing Jiang, Bo Li, and Liyuan Yu. "Estimating permeability of porous media based on modified Hagen–Poiseuille flow in tortuous capillaries with variable lengths." *Microfluidics and Nanofluidics* 20, no. 8 (2016): 120.
- Liu, Shijie, and Jacob H. Masliyah. "Single fluid flow in porous media." *Chemical Engineering Communications* 148, no. 1 (1996): 653-732.
- Liu, Yongge, Jian Hou, Qingliang Wang, Jingyao Liu, Lanlei Guo, Fuqing Yuan, and Kang Zhou. "Flow of Preformed Particle Gel through Porous Media: A Numerical Simulation Study Based on the Size Exclusion Theory." *Industrial & Engineering Chemistry Research* 56, no. 10 (2017): 2840-2850.
- Majumder, Mainak, Nitin Chopra, and Bruce J. Hinds. "Mass transport through carbon nanotube membranes in three different regimes: ionic diffusion and gas and liquid flow." *ACS nano* 5, no. 5 (2011): 3867-3877.
- Majumder, Mainak, Nitin Chopra, Rodney Andrews, and Bruce J. Hinds. "Nanoscale hydrodynamics: enhanced flow in carbon nanotubes." *Nature* 438, no. 7064 (2005): 44-44.

- Matin, Mohammad Reza, Hamid Reza Mirdamadi, and Mostafa Ghayour. "Effects of nonlocal elasticity and slip condition on vibration of nano-plate coupled with fluid flow." *Physica E: Low-dimensional Systems and Nanostructures* 48 (2013): 85-95.
- Matyka, Maciej, Arzhang Khalili, and Zbigniew Koza. "Tortuosity-porosity relation in porous media flow." *Physical Review E* 78, no. 2 (2008): 026306.
- Mavko, Gary, and Amos Nur. "The effect of a percolation threshold in the Kozeny-Carman relation." *Geophysics* 62, no. 5 (1997): 1480-1482.
- Mirramezani, Mehran, and Hamid Reza Mirdamadi. "The effects of Knudsen-dependent flow velocity on vibrations of a nano-pipe conveying fluid." *Archive of applied mechanics* 82, no. 7 (2012): 879-890.
- Mobedi, Moghtada, Murat Barisik, and A. Nakayama. "16 Heat and Fluid Flow of Gases in Porous Media with Micropores: Slip Flow Regime." (2016).
- Mujeebu, M. Abdul, M. Z. Abdullah, MZ Abu Bakar, A. A. Mohamad, and M. K. Abdullah. "Applications of porous media combustion technology—a review." *Applied Energy* 86, no. 9 (2009): 1365-1375.
- Nakayama, Akira. *PC-aided numerical heat transfer and convective flow*. CRC press, 1995.
- Naraghi, Morteza Elahi, and Farzam Javadpour. "A stochastic permeability model for the shale-gas systems." *International Journal of Coal Geology* 140 (2015): 111-124.
- Navier, C. L. M. H. "Mémoire sur les lois du mouvement des fluides." *Mem. Acad. Sci. Inst. Fr* 6, no. 1823 (1823): 389-416.
- Neto, Chiara, Drew R. Evans, Elmar Bonaccorso, Hans-Jürgen Butt, and Vincent SJ Craig. "Boundary slip in Newtonian liquids: a review of experimental studies." *Reports on Progress in Physics* 68, no. 12 (2005): 2859.
- Ou, Jia, Blair Perot, and Jonathan P. Rothstein. "Laminar drag reduction in microchannels using ultrahydrophobic surfaces." *Physics of fluids* 16, no. 12 (2004): 4635-4643.
- Ozgunus, Turkuler, Moghtada Mobedi, and Unver Ozkol. "Determination of Kozeny constant based on porosity and pore to throat size ratio in porous medium with rectangular rods." *Engineering Applications of Computational Fluid Mechanics* 8, no. 2 (2014): 308-318.
- Payatakes, A. C., R. Rajagopalan, and Chi Tien. "Application of porous media models to the study of deep bed filtration." *The canadian journal of chemical engineering* 52, no. 6 (1974): 722-731.
- Phillip, William A., Javid Rzayev, Marc A. Hillmyer, and E. L. Cussler. "Gas and water liquid transport through nanoporous block copolymer membranes." *Journal of Membrane Science* 286, no. 1 (2006): 144-152.

- Qin, Xingcai, Quanzi Yuan, Yapu Zhao, Shubao Xie, and Zhongfan Liu. "Measurement of the rate of water translocation through carbon nanotubes." *Nano letters* 11, no. 5 (2011): 2173-2177.
- Ramos-Alvarado, Bladimir, Satish Kumar, and G. P. Peterson. "Hydrodynamic slip in silicon nanochannels." *Physical Review E* 93, no. 3 (2016): 033117.
- Rashidi, Vahid, Hamid Reza Mirdamadi, and Ebrahim Shirani. "A novel model for vibrations of nanotubes conveying nanoflow." *Computational Materials Science* 51, no. 1 (2012): 347-352.
- Rezaee, M. R., A. Jafari, and E. Kazemzadeh. "Relationships between permeability, porosity and pore throat size in carbonate rocks using regression analysis and neural networks." *Journal of Geophysics and Engineering* 3, no. 4 (2006): 370.
- Rodriguez, E., F. Giacomelli, and A. Vazquez. "Permeability-porosity relationship in RTM for different fiberglass and natural reinforcements." *Journal of composite materials* 38, no. 3 (2004): 259-268.
- Rogers, Benjamin J., and Mary J. Wirth. "Slip flow through colloidal crystals of varying particle diameter." *ACS nano* 7, no. 1 (2012): 725-731.
- Roy, Pratanu, N. K. Anand, and Debjyoti Banerjee. "Liquid slip and heat transfer in rotating rectangular microchannels." *International Journal of Heat and Mass Transfer* 62 (2013): 184-199.
- Saada, Mebrouk Ait, Salah Chikh, and Antonio Campo. "Analysis of hydrodynamic and thermal dispersion in porous media by means of a local approach." *Heat and mass transfer* 42, no. 11 (2006): 995-1006.
- Schmatko, Tatiana, Hubert Hervet, and Liliane Leger. "Friction and slip at simple fluid-solid interfaces: the roles of the molecular shape and the solid-liquid interaction." *Physical review letters* 94, no. 24 (2005): 244501.
- Sendner, Christian, Dominik Horinek, Lyderic Bocquet, and Roland R. Netz. "Interfacial water at hydrophobic and hydrophilic surfaces: Slip, viscosity, and diffusion." *Langmuir* 25, no. 18 (2009): 10768-10781.
- Serra, O. "Fundamentals of Well-Log Interpretation (Vol. 1): The Acquisition of Logging Data: Dev." *Pet. Sci. A* 15 (1984).
- Sofos, Filippou, Theodoros E. Karakasidis, and Antonios Liakopoulos. "Parameters affecting slip length at the nanoscale." *Journal of Computational and Theoretical Nanoscience* 10, no. 3 (2013): 648-650.
- Sokhan, V. P., D. Nicholson, and N. Quirke. "Fluid flow in nanopores: an examination of hydrodynamic boundary conditions." *The Journal of Chemical Physics* 115, no. 8 (2001): 3878-3887.
- Suk, M. E., and N. R. Aluru. "Molecular and continuum hydrodynamics in graphene nanopores." *RSC Advances* 3, no. 24 (2013): 9365-9372.

- Sun, Jie, Ya Ling He, Wen Quan Tao, John W. Rose, and Hua Sheng Wang. "Multi-scale study of liquid flow in micro/nanochannels: effects of surface wettability and topology." *Microfluidics and nanofluidics* 12, no. 6 (2012): 991-1008.
- Thies-Weesie, Dominique ME, and Albert P. Philipse. "Liquid permeation of bidisperse colloidal hard-sphere packings and the Kozeny-Carman scaling relation." *Journal of colloid and interface science* 162, no. 2 (1994): 470-480.
- Thomas, John A., Alan JH McGaughey, and Ottoleo Kuter-Arnebeck. "Pressure-driven water flow through carbon nanotubes: insights from molecular dynamics simulation." *International Journal of Thermal Sciences* 49, no. 2 (2010): 281-289.
- Thomas, John A., and Alan JH McGaughey. "Reassessing fast water transport through carbon nanotubes." *Nano letters* 8, no. 9 (2008): 2788-2793.
- Thomas, Michael, Ben Corry, and Tamsyn A. Hilder. "What have we learnt about the mechanisms of rapid water transport, ion rejection and selectivity in nanopores from molecular simulation?" *Small* 10, no. 8 (2014): 1453-1465.
- Tretheway, Derek C., and Carl D. Meinhart. "Apparent fluid slip at hydrophobic microchannel walls." *Physics of fluids* 14, no. 3 (2002): L9-L12.
- Valdes-Parada, Francisco J., J. Alberto Ochoa-Tapia, and Jose Alvarez-Ramirez. "Validity of the permeability Carman-Kozeny equation: a volume averaging approach." *Physica A: Statistical Mechanics and its Applications* 388, no. 6 (2009): 789-798.
- Voronov, Roman S., Dimitrios V. Papavassiliou, and Lloyd L. Lee. "Boundary slip and wetting properties of interfaces: correlation of the contact angle with the slip length." *The Journal of chemical physics* 124, no. 20 (2006): 204701.
- Voronov, Roman S., Dimitrios V. Papavassiliou, and Lloyd L. Lee. "Slip length and contact angle over hydrophobic surfaces." *Chemical physics letters* 441, no. 4 (2007): 273-276.
- Wang, Xiukun, and James J. Sheng. "Effect of low-velocity non-Darcy flow on well production performance in shale and tight oil reservoirs." *Fuel* 190 (2017): 41-46.
- Woudberg, S., and J. P. Du Plessis. "Predicting the permeability of very low porosity sandstones." *Transport in Porous Media* 73, no. 1 (2008): 39-55.
- Wu, Jinsui, and Boming Yu. "A fractal resistance model for flow through porous media." *International journal of heat and mass transfer* 50, no. 19 (2007): 3925-3932.
- Wu, Jinsui, Dezhi Hu, Wenjun Li, and Xin Cai. "A review on non-darcy flow— forchheimer equation, hydraulic radius model, fractal model and experiment." *Fractals* 24, no. 02 (2016): 1630001.
- Wu, Jinsui, Jianchao Cai, Dongyun Zhao, and Xuexi Chen. "An analysis of mine water inrush based on fractal and non-Darcy seepage theory." *Fractals* 22, no. 03 (2014): 1440008.

- Xiao, Boqi, Jintu Fan, and Feng Ding. "Prediction of relative permeability of unsaturated porous media based on fractal theory and Monte Carlo simulation." *Energy & Fuels* 26, no. 11 (2012): 6971-6978.
- Xiao, Boqi, Jintu Fan, and Feng Ding. "Prediction of relative permeability of unsaturated porous media based on fractal theory and Monte Carlo simulation." *Energy & Fuels* 26, no. 11 (2012): 6971-6978.
- Xiao, Boqi, Xing Tu, Wen Ren, and Zongchi Wang. "Modeling for hydraulic permeability and kozeny–Carman constant of porous nanofibers using a fractal approach." *Fractals* 23, no. 03 (2015): 1550029.
- Xu, Jinliang, and Yuxiu Li. "Boundary conditions at the solid–liquid surface over the multiscale channel size from nanometer to micron." *International Journal of Heat and Mass Transfer* 50, no. 13 (2007): 2571-2581.
- Xu, Peng, and Boming Yu. "Developing a new form of permeability and Kozeny–Carman constant for homogeneous porous media by means of fractal geometry." *Advances in water resources* 31, no. 1 (2008): 74-81.
- Xu, Peng. "A discussion on fractal models for transport physics of porous media." *Fractals* 23, no. 03 (2015): 1530001.
- Yang, Chen, Qinglian Wang, Akira Nakayama, and Ting Qiu. "Effect of temperature jump on forced convective transport of nanofluids in the continuum flow and slip flow regimes." *Chemical Engineering Science* 137 (2015): 730-739.
- Yang, Shanshan, Mingchao Liang, Boming Yu, and Mingqing Zou. "Permeability model for fractal porous media with rough surfaces." *Microfluidics and Nanofluidics* 18, no. 5-6 (2015): 1085-1093.
- Yang, Xiaofan, and Zhongquan C. Zheng. "Effects of channel scale on slip length of flow in micro/nanochannels." *Journal of Fluids Engineering* 132, no. 6 (2010): 061201.
- Yasuoka, Haruka, Ryo Takahama, Masayuki Kaneda, and Kazuhiko Suga. "Confinement effects on liquid-flow characteristics in carbon nanotubes." *Physical Review E* 92, no. 6 (2015): 063001.
- Yeh, Kuan-Yu, Kuan-Hung Cho, and Li-Jen Chen. "Preparation of Superhydrophobic Surfaces of Hierarchical Structure of Hybrid from Nanoparticles and Regular Pillar-Like Pattern†† Part of the" *Langmuir* 25th Year: Wetting and superhydrophobicity" special issue." *Langmuir* 25, no. 24 (2009): 14187-14194.
- Yen, Tsu-Hsu, and Chyi-Yeou Soong. "Effective boundary slip and wetting characteristics of water on substrates with effects of surface morphology." *Molecular Physics* 114, no. 6 (2016): 797-809.
- Yen, Tsu-Hsu. "Effects of wettability and interfacial nanobubbles on flow through structured nanochannels: an investigation of molecular dynamics." *Molecular Physics* 113, no. 23 (2015): 3783-3795.

- Zhang, Chengbin, and Yongping Chen. "Slip behavior of liquid flow in rough nanochannels." *Chemical Engineering and Processing: Process Intensification* 85 (2014): 203-208.
- Zhang, Zhiqiang, Yongmin Shi, He Li, and Wenqi Jin. "Experimental study on the pore structure characteristics of tight sandstone reservoirs in Upper Triassic Ordos Basin China." *Energy Exploration & Exploitation* 34, no. 3 (2016): 418-439.